学位申請論文

金尾　政紀

Study on Shear Wave Structure for the Crust in the Lützow-Holm Bay Region, East Antarctica

Masaki KANAO

c/o : National Institute of Polar Research
Kaga 1-9-10, Itabashi-ku, Tokyo 173
TEL : +81-3-3962-3275
FAX : +81-3-3962-5741
E-mail : *kanao@nipr.ac.jp*

CONTENTS

Abstract: Crustal structure in the Lützow-Holm Bay region (LHB), East Antarctica, was investigated by using seismological waveform data obtained from refraction experiments and local telemetry networks, together with broadband seismographs at Syowa Station (SYO; 69.0°S, 39.6°E). Crustal models for explaining shear waves' propagation in this region were calculated, in particular concerning crustal heterogeneity. At first, local earthquakes detected by telemetry networks in 1987-1989 were analyzed by shifting the lapse time of coda part of *S*-waves and a one-dimensional crustal attenuation (Q_S) model characterized by weak attenuation and strong frequency dependence of Q_S was obtained in 1-24 Hz. Next, radial receiver functions developed from teleseismic *P*-waveforms of broadband seismographs at SYO in 1990-1993 were inverted for the crustal velocity models of shear waves, in which each layer's thickness was taken to be 1-2 km. Lateral heterogeneity was investigated by comparing the velocity models in the four backazimuth groups. Velocity changes were recognized as a sharp Moho at 36-38 km depth in the continental areas in 50°-160°; in contrast we revealed smooth variation of crustal velocities together with transitional Moho in the bay backazimuths in 210°-360°. Continental velocity models in the two different facies terrains were also related to the linking velocity to lithology by laboratory data. In order to compare the shear wave crustal models with reflected waves in the crust, refraction data on the Mizuho Plateau were re-analyzed. The reflective layers are at depths of 24-45 km, which mainly correspond to the lower crust, with a well known relation to the Bouguer gravity anomalies. The Moho depth estimated from the Bouguer anomalies also indicated a seaward dipping Moho from 40 km in the coastal area to 48 km beneath Dome-F (77.4°S, 39.6°E). Crustal anisotropy for shear waves found by splitting analysis of Moho *Ps* phases was quantified by the fastest direction in N133°E, which is perpendicular to the upper mantle anisotropy from *SKS* phases. By comparing the crustal shear wave models with other geophysical and geological evidence, the reasonable crustal evolution in LHB is explained in relation with the regional metamorphism at 500 Ma and the last break-up of Gondwana at 150 Ma.

1. Introduction

Seismological studies of the crustal structure in and around Antarctica started from 1957 during the International Geophysical Year (IGY). The earth's interior beneath Antarctica was first investigated by surface wave analyses (e.g., Evison et al., 1960; Kovach and Press, 1961; Knopoff and Vane, 1979). In recent years, tomographic models of phase velocity within Antarctica and the surrounding oceans were obtained from analyses of 213 paths from the broadband seismographs of GEOSCOPE stations in the southern hemisphere (Rouland and Roult, 1992). Extended analyses were conducted to obtain more precise models by use of 399 paths (Roult et al., 1994). East Antarctica, in particular around the Napier Complex, Enderby Land, has phase velocity higher by 6 per cent than the other regions of Antarctica, where the oldest metamorphic rocks in 400 Ma were found in the Archean crust (e.g., Ellis, 1983, Black et al., 1987). This oldest craton has been found to have a spatial wavelength about 500 km from the above surface wave analyses. The root thickness of the Archean craton attains the depth of 250 km as found by evidence of high velocity anomalies from tomographic studies (Polet and Anderson, 1995).

The crustal velocities beneath the Antarctic continent have also been investigated mainly by refraction explosion experiments (reviewed by Bentley, 1983; Kadmina et al., 1983). Geotransects around the Lützow-Holm Bay region (LHB), East Antarctica, including seismic velocity models from refraction experiments have been summarized by Kaminuma et al. (1991). However, the reflective patterns of the crust are also useful information for research on the evolution of the Antarctic continent. The recent reflection studies in the Precambrian crust indicate the existence of ancient events for continental collisions and/or rifting with no association with the present plate motions (Goleby et al., 1990; BABEL-Working Group, 1990; Green et al., 1989). Although the results of coincident seismic reflection/refraction studies of the continental crust have been compiled (Mooney and Brocher et al., 1987), detection of the reflected waves from the lower crust in Antarctica has not been done yet. Reflective explosive surveys on land reaching to the lower crust have not been carried out, so that the deep crustal reflection profiles in Antarctica remains a scientific frontier. It is important to study the crustal structure in Enderby Land and Eastern Queen

Maud Land, because there are some ancient orogens of continental crust from Archean to Phanerozoic ages.

Although the crustal structures in East Antarctica have been investigated by the above seismological approaches, they do not have enough spatial resolution for the obtained crustal velocity structures. The spatial resolution of the surface wave analyses is several tens of kilometers. In contrast, the vertical variations of the velocity structures by the refraction analyses are on sales of only a few kilometers, as in the case of seismic explosion experiments on Mizuho Plateau (Ikami et al., 1984; Ito and Ikami, 1984). It is, therefore, necessary to obtain more precise crustal models of the Antarctic continent including some geophysical parameters, such as seismic velocity, quality factor, Poisson's ratio and density by use of several seismological and geodetic approaches applying recent digital seismic waveforms instead of surface wave and/or travel-time data.

The geological setting in Eastern Queen Maud Land and Western Enderby Land, East Antarctica is shown in Fig. 1 (modified from Motoyoshi et al., 1989). Syowa Station (SYO; 69.0°S, 39.6°E) is situated on the Lützow-Holm Complex (LHC), where the regional metamorphism occurred in the late-Proterozoic to Paleozoic (Hiroi, et al., 1991; Shiraishi, et al., 1992, 1994; Motoyoshi et al., 1989). Metamorphic grade increases progressively from the Prince Olav Coast region (east) to the Soya Coast region (west) and the maximum thermal axis lies at southern Lützow-Holm Bay in the NNW-SSE direction. LHC was under compressional stress perpendicular to the thermal axis during this metamorphism in 500 Ma as in the Cambrian orogenic belt. In 150 Ma, there was the break-up of the Gondwana super-continent in relation to the Antarctica/Australia-India rifting (e.g., Anderson, 1994; Storey, 1995; Hill, 1991) when LHC was in the condition of extentional stress to induce the uplifting of mantle material and underplating.

In this paper, the crustal structure in LHB was investigated by making use of the currently available seismological waveform data to obtain insight into the fine crustal models, in particular, concerning heterogeneity. The evolution of LHC is also discussed as one of the target field regions in the East Antarctic shield. At first, local earthquakes recorded on the telemetry networks in 1987-1989 (Akamatsu et al., 1989, 1990) were analyzed by varying the lapse time to coda generation of S-waves to obtain a one-dimensional crustal attenuation (Q_S) model. Next, the radial receiver

functions developed from teleseismic *P*-waveforms recorded on the broadband seismographs at SYO from 1990 to 1993 are inverted for the shear wave velocity models of the crust and uppermost mantle. The one-dimensional velocity models for shear waves were obtained with layers of 1-2 km thickness in the four backazimuth groups. A one-dimensional Q_S model from the coda-Q inversion was used as the initial depth-dependent parameter. The shear wave structures obtained by the waveform analyses are discussed, focusing on the lateral heterogeneity and anisotropy of the azimuthal distribution. The obtained shear wave crustal structures were compared with the reflection section on the Mizuho Plateau, eastern continental area in LHB (Ito and Kanao, 1995). Crustal thickness was also investigated in association with the gravity anomalies along the inland traverse routes on the Mizuho Plateau. Shear wave anisotropy in the crust is also estimated by analyzing the splitting of Moho *Ps* phases observed in the receiver functions. Then, the crustal models obtained by these seismological analyses are compared with other geophysical and geological evidence in relation to the evolution of LHC. Fig. 2 summarizes the location of areas studied in LHB by using a seismological approach.

2. Crustal attenuation model for shear waves

2.1. Coda Q by local seismic networks in LHB

Attenuation properties of seismic waves in the lithosphere have been studied by the analysis of decay of coda amplitudes with time. The coda parts of *S*-waves for local earthquakes are considered to consist mainly of *S*-waves scattered (reflected, refracted and diffracted) by random inhomogeneity in the lithosphere (Aki, 1969; Aki and Chouet, 1975). The attenuation factor determined by the time decay of coda amplitude is called the coda Q (Q_C). On the basis of the observed Q_C and attenuation factor for the *S*-waves (Q_S), Q_C is assumed to reflect the averaged Q_S within an ellipsoid of the scattering medium in the lithosphere. Regional differences in Q_C have also been determined in relation to tectonics and local seismicity (e.g., Akamatsu, 1980; Akamatsu et al.,

1995; Pulli, 1984; Sato, 1986; Eck, 1988; Correig et al., 1990; Nishigami et al., 1990; Kanao and Ito, 1990, 1991, 1992) together with the frequency exponent n in the formula $Q = Q_0 f^n$, where f is frequency in Hz. For example, Jin et al. (1985) investigated the regional variations in Q_C for the oceanic lithosphere, finding that the younger oceanic lithosphere has a higher n value than the older one, which is similar to the active continental regions with higher n values. Thus the Q_C and n values provide an efficient way to determine the attenuation characteristics and their relation to seismo-tectonics in the studied area. Therefore, it is important to determine the attenuation model in the stable shield region in East Antarctica in order to compare with other tectonic regions.

In LHB, a local telemetry seismic network along the Soya Coast was operated from June 1987 to October 1989 to study local seismicity and the characteristics of wave propagation (Akamatsu et al., 1989, 1990). The networks consist of stations of spacing about 15 km along the Soya Coast and a smaller tripartite array of spacing about 1 km around SYO. The attenuation factor by coda part of S-waves (Q_C) in LHB was determined (Akamatsu, 1991) on the basis of the single isotropic scattering model applied to the coda part of S-waves for six shallow earthquakes observed with the above local networks. The Q_C was estimated in the frequency range of 1-24 Hz for the lapse time windows of 20-210 s. The Q_C at low frequency around 1 Hz is about 125 at the lapse time of 30 s, which is larger by a factor of 1.5 times than that of tectonic active regions such as Kinki district, Japan (Akamatsu, 1980; Kanao and Ito, 1990; 1991; etc.). Moreover, Q_C is the largest about 3000 at the lapse time of 30 s in the regional lithosphere at higher frequency range of 24 Hz. The strong frequency dependence of Q_C was also found about the value of 0.93, particularly for the deep lithosphere, comparing to the averaged values about 0.79 for 20-85 s lapse times ranges in the Kinki district (Kanao and Ito, 1990). A scattering energy loss occurred for shear waves in the crustal heterogeneity corresponding to the wavelength of 1 Hz, however, the intrinsic absorption in the whole frequency band is small as a stable shield region.

2.2. Data and method

In this analysis, five earthquakes observed by the above local telemetry networks were analyzed varying the lapse time to coda generation from 20 s to 70 s for each waveform trace in

order to obtain a one-dimensional layered model of Q_S for the lithosphere. Ninety-two waveform traces of the five earthquakes recorded at six stations (large and small tripartites) were analyzed to obtain Q_C. The radius of the scattering sphere affecting the coda wave generation for the maximum lapse time of 70 s is restricted to the lithosphere at depth of about 120 km, which is indicated by the circle with its center at SYO in Fig. 2. The scattering area covers almost all of LHB, from the Prince Olav Coast in the north to the Shirase Glacier in the south. For the shortest lapse time of 20 s, the volume within the crust makes the main contribution to Q_C In contrast, the volume of the uppermost mantle mostly affects Q_C for a long lapse time of 70 s.

For calculation of the layered Q_S model in the lithosphere, single isotropic scattering and spatially uniform distribution of scattering strength are assumed. The Q_S model was estimated by the inversion technique using the Marquardt method (Kosuga, 1992). In the following analysis, Q_C is considered to be the averaged Q_S within the scattering ellipsoid whose dimension is determined by the lapse time. Q_C increases rapidly in the short lapse time range and gradually increases in the large lapse time range. We interpret this observation as an indication of the depth variation for Q_S in the lithosphere. For a large lapse time range, the scattering ellipsoid is approximated by a sphere and is divided into 15 layers with constant Q_S We also assumed that the S-wave velocity is a constant 3.5 km/s within the scattering area. In order to minimize the estimation errors, the solution is constrained to not deviate significantly from the initial values. The initial values of Q_S for all layers are determined by forward modeling of trial-and-error estimation. The P-velocity model from the explosive refraction experiments on the Mizuho Plateau (Ikami et al., 1984) is adopted to constrain the layer thickness.

2.3. Inversion and results

The results of coda Q inversion in LHB are shown in Fig. 3. In the previous study (Kanao and Akamatsu, 1995), Q_S models were obtained in the three frequency bands of 4, 8 and 16 Hz. In this study, since three frequency bands were added, six bands of 1, 2, 4, 8, 16 and 24 Hz were re-analyzed. Observed and calculated Q_C are plotted as a function of lapse time for six frequency bands. We obtained enough data of good S/N ratio for all frequency bands except for those of 1

Hz at lapse time longer than 40 s. The mean values of observed Q_C for each lapse time window are shown by broken lines. On the other hand, those calculated on the assumption of a one-dimensional Q_S model are shown by solid lines. For most of the frequency bands, calculated Q_C have larger values in the short lapse time range less than around 50 s and take smaller values than the averaged Q_C in longer lapse times.

Fig. 4 shows an inverted one-dimensional Q_S model from the surface layer to the depth of 60 km. The Q_S in LHB is larger by a factor of 1.2-1.4 than those of typical values in the tectonic active island arc regions (Akamatsu, 1980; Kanao and Ito, 1990, 1992) for all frequency bands. The frequency dependence of Q_S is also large in LHB, which is attributed to high frequency-exponent (n) values. This shows that the small scale heterogeneity corresponding to the wavelength of the high frequency band is weak. The Q_S model from coda Q inversion is attributed to the high Q in the uppermost mantle which implies a thick lithosphere in LHB. High Q_S near the surface in LHB is due to the lack of a sedimentary layer with low velocity. All these characteristics of large Q_S values indicate that LHB, representative of a stable shield region, has a homogeneous lithosphere for the propagation of S-waves than in active tectonic regions, particularly in the high frequency range.

3. Teleseismic receiver functions

3.1. Broadband seismograms at Syowa Station

Together with the three-component short- and long-period seismometers from 1967 (Kaminuma et al., 1968), broadband seismic observations with a three-component Streckeisen Seismometer (STS-1V, -1H) (Wielandt and Streckeisen, 1982) have been carried out at SYO since April 1989. The wide dynamic-range recording system for the BRoadBand (BRB) velocity output signal was started in May 1990 (Nagasaka et al., 1992). In the course of the observations, many kinds of performance test of STS-seismograph in low temperature were conducted in the low

temperature laboratory of the National Institute of Polar Research, Japan (Kanao and Kaminuma, 1994a). Details of the recording system for the BRB seismograph at SYO are given by Kanao and Kaminuma (1994b). The waveform data are after the BRB signals at the sampling frequency of 10 Hz with 24-bit resolution.

The earthquake detectability of teleseismic events at SYO in the last seven years were reported and the high-quality waveform data have been provided via the Internet (Kanao and Kaminuma, 1995; Kanao et al., 1995). SYO plays an important role as the seismological station of its location in the high southern latitude in the Japanese Pacific Orient SEIsmic Digital Observation Network (POSEIDON) (Tsuboi, 1995), which is the Japanese contribution to the research program of Federation of Digital Seismographic Networks (FDSN). Some seismological research on the earth's interior in and around the Antarctic Plate has recently been conducted by use of the broadband waveform data at SYO.

3.2. Observed receiver functions

Recently, the broadband digital seismographs have been used to determine the shear velocity structure of the crust and uppermost mantle beneath isolated seismic stations (e.g., Owens et al., 1984; Owens and Zandt, 1985; Owens, 1987; Visser and Paulssen, 1993; Lupei et al., 1994; Kind et al., 1995). In this section, the radial receiver functions developed from teleseismic *P*-waveforms recorded with the broadband seismographs at SYO from May 1990 to January 1993 are inverted to infer the crustal shear velocity models in LHB. Since the receiver functions are sensitive to *P*-to-*S* conversions through the interfaces beneath a recording station, the inversion result gives information of the shear velocity structure (e.g., Owens et al., 1984). In order to produce the observed receiver functions, the source-equalization method (Langston, 1979) is adopted to the *P*-waveforms of teleseismic events recorded on the broadband seismographs. Crustal response of the earth structure was isolated from that of the instrument and effective seismic source function. Observed receiver functions are obtained by the following parameter setting and analytical procedures. First, noises longer than 0.10-0.20 Hz are suppressed by high-pass-filtering. Then the vertical component is deconvolved from the radial component by a spectral division, applying

the water level parameter which controls the smallest spectral amplitude allowable for the vertical component. A Ganssian high-cut filter of 1 Hz is also applied to suppress high frequency noises; it is sensitive to about 1 km layers thickness. The water level parameter is also varied depending on the signal-to-noise ratio of each trace. The data length of receiver functions is set to 40 s from the *P*-arrival, in order to eliminate contamination of the other large phases such as *PP*, which have different slowness from that of direct *P*-waves.

A total of 80 earthquakes with sufficient signal-to-noise ratios are used to obtain the observed receiver functions (Table 1 and Fig. 5). Hypocentral distances are within 70°-90° that produce the similar incident angle of 20°-25° for the direct *P*-arrivals. Backazimuth range is divided into four groups of 50°-100°, 120°-160°, 210°-250° and 300°-360°, respectively. Location of SYO and the target region of the horizontal spacing about 100 km are presented in Fig. 2. Lateral heterogeneity is identified by examining the variations of the vertical structures in the different backazimuths. For example, as seen in Fig. 2, the rays from the backazimuths of 50°-100° and 120°-160° travel mainly through the continental area beneath the ice sheet on the Mizuho Plateau. Rays of 210°-250° and 300°-360° propagate mainly within the Lützow-Holm Bay area. In the continental area, the group of backazimuth 50°-100° mainly belongs to the transitional zone between amphibolite facies and granulite facies. On the other hand, the 120°-160° backazimuth group is within the granulite facies. The horizontal extent which affects the generation of the receiver function is estimated to be about 100-150 km for each backazimuth.

In the inversion procedure described in *4.1*, we used the weighting-stacked receiver functions to determine shear velocity models in the neighboring backazimuth groups and incident angle. Weighting-center backazimuths for stacking are 80°-90°, 140°-150°, 240°-250° and 350°-360°, respectively, where the maximum number of original traces are used in each group (see Table 1). Fig. 6 presents an example of the weighting-stacked radial receiver function together with the 26 original traces in the backazimuth of 50°-100°. The incoherent noises can be suppressed by stacking, while the coherent signals were enhanced as seen around 1.5 s, 2.5 s, 4 s and 11 s, *etc.* There are several noticeable later phases after the *P*-arrival for all the backazimuths. The strong amplitudes of later phases around 4–5 s, for example, are explained by the direct *P*-to-*S* converted phases at the Moho (Moho *Ps* phases). There are also several large amplitudes in later phases

around 8-9 s and 14-15 s, which are considered to be composed of the reverberations within the crust. We took a correlation between the direct *P*-phases and later phases in the coda part of *P*-waves until 10 s for all the radial receiver functions used in this study. Fig. 7 shows the histogram of delay time from *P*-arrivals of the strong amplitudes having positive correlation greater than 0.2. Two main peaks are found around 1 s and 4 s after *P*-arrivals in the histogram; they are considered to be *Ps* phases from discontinuities in the upper-to-middle crust and Moho, respectively.

4. Lateral variation in shear velocity models

4.1. Inversion and model dependence

A time domain inversion (Shibutani, 1993) is applied to the weighting-stacked radial receiver functions up to 30 s from the *P*-arrival to determine the velocity model for each backazimuth group. A smoothness constraint in the inversion is implemented by minimizing a roughness norm of the velocity model (Ammon et al., 1990). After examining the trade-off curves between the model roughness and waveform-fit residuals, we selected the most suitable pair of the above parameters. The necessary number of iterations, up to 30-times, was conducted in the inversion procedures in order to reduce the waveform-fit residuals to the allowable extent and the most stable solutions were adopted as the final models. The *P*-wave velocity model determined by the refraction experiments in the northern Mizuho Plateau in 1979-1981 (Ikami et al., 1984) is adopted as an initial velocity model with the assumption that the V_P/V_S is 1.73 in the crust and 1.80 in the uppermost mantle, respectively. Difference in the starting velocity models within +-1% have a less affect on the inverted shear models concerning lithologic velocities discussed in Chapter 6. The obtained shear wave velocity models consist of 32 layers with thickness about 1-2 km, because all the observed receiver functions are created after 1 Hz Gaussian low-pass-filter, which are most sensitive to velocity discontinuities of 1 km thickness. In the inversion procedure, the shear wave velocity beneath 60 km was fixed to be 4.47 km/s. Lower- and upper-limits for the shear wave velocity in

each layer are introduced by the least square method with linear inequality constraints by Lawson and Hanson (1974). The above model parameters in the inversion procedure are summarized in Table 2.

In order to investigate the dependence on the initial model for quality factor, shear velocity models were compared with the different one-dimensional Q_S model of 1, 2 and 4 Hz in the 50°-100° backazimuths (Fig. 8). There is an ambiguity for the different Q_S models, particularly in determining the lower crustal shear velocities. The initial Q_S values, however, have a less affect on producing a final model in the inversion comparing to the variation of initial shear velocity. The crustal attenuation model for shear wave (Q_S) is finally adopted after the cases of 1 Hz, because the sensitive frequency for the applied Gaussian high-pass filter is about the same frequency. The final fine models are obtained as 32 layers with 1-2 km thickness. The velocity models in the lower crustal depth will be discussed in Chapter 5 in relation to the crustal reflectivity.

4.2. Azimuthal difference in shear velocity models

Shear velocity models obtained by the receiver function inversion are discussed, focusing on the lateral heterogeneity by detailed comparison of the azimuthal dependence around SYO. As for the general features of the crustal velocities in all the backazimuths, the averaged velocities of the crust range from 3.0 to 3.8 km/s. These are consistent with the typical velocity models in East Antarctica determined by the previous surface wave analyses (e.g., Evison et al., 1960; Kovach and Pres, 1961; Dewart and Toksöz, 1965). The shear velocities of the uppermost mantle range from 4.1 to 4.8 km/s in all the backazimuths; the large fluctuations may be associated with the depth variations in velocities and complicated crust-to-mantle structures. As pointed out by Ammon et al. (1990), there may also be a possibility of trade-off between Moho depth and average velocity of the crust in the receiver function inversion.

Shear wave velocity models down to 60 km depth by the receiver function inversion in the four backazimuth groups are presented in Figs. 9a-12a with synthetic receiver functions of the corresponding backazimuths in Figs. 9b-12b. As for the continental backazimuths in 50°-100° and 120°-160°, velocity-depth curves vary, for example showing patterns of high, low and high velocity

lamination near the surface 5 km layers, in the upper crust and in the middle crust, respectively. These characteristic velocity variations are presumably associated with the corresponding large amplitudes of the radial receiver functions around 2-3 s as shown in Figs. 9b, 10b. The crustal velocity increases with depth in the backazimuths of 50°-100°, while a small increase is found in the backazimuth of 120°-160°. In contrast, velocity models in the bay backazimuths of 210°-250° (Fig. 11a) and 300°-360° (Fig. 12a) resulted in no strong velocity fluctuations in the upper and middle crust. These smooth velocity models in the bay backazimuths are also explained by the small amplitudes of receiver functions in the first 4 s after *P*-arrival (see Figs. 11b, 12b).

The structures around the Moho depth also indicate several characteristic velocity patterns, such as sharp discontinuity beneath the thin-transitional lower crust, in the continental backazimuths of 50°-100° and 120°-160° The Moho depth of around 37 km in these backazimuths is about 3 km shallower than that from previous refraction experiments on the Mizuho Plateau (Ikami et al., 1984). This sharp Moho is consistent with large amplitudes of Moho *Ps* phases around 4 s in the receiver functions (see Figs. 9b, 10b). On the other hand, the broad-transitional lower crust and Moho are obtained in the bay backazimuths of 210°-250°, 300°-360° with the range of 35-45 km depth. Otherwise, the Moho depth can be shallow around 35 km, if we assume that the upper part of the crust-to-mantle transitional zone in the Moho, which correlates to faster arrivals of Moho *Ps* phases around 3.7-3.8 s in the bay backazimuths (Figs. 11b, 12b) than in the continental azimuths. The crustal thickness of 35 km in the bay backazimuths is the characteristic value as the typical continental margins, that is, the transition zone between the continental and the normal oceanic crust. The Moho depth might also become deeper, about 5-7 km, from the north backazimuths (50°-100° and 300°-360°) to the south (120°-160° and 210°-250°). This deepening of the Moho presumably must relate to the southward dipping structure in the continental margin.

5. Lower crustal reflectivity

5.1. Reflection analysis of the 1979-1981 refraction experiment data

An explosion in Lützow-Holm Bay (SHOT 19 in Fig. 2) with 3000 kg of explosives during the 1979-1981 seismic refraction experiments (Ikami et al., 1984; Ito and Ikami, 1984) gave well-recorded seismic waves at all 27 stations along the 300 km profile from the Soya Coast to the inland Mizuho Plateau. From the analyses of travel-time and comparison of observed seismograms with the synthetic ones, Moho depth was determined to be about 40 km with the *P*-wave velocities in the surface layer, middle crust, lower crust and uppermost mantle of 6.0, 6.4, 6.9 and 7.8 km/s, respectively. The evidence of high velocity in the surface layer and in the lower crustal layers is typical of the Precambrian crust (e.g., Christensen and Mooney, 1995; Rudnick and Fountain, 1995).

The above seismic refraction data were re-analyzed to detect a rough image of reflected waves from the lower crust (Ito and Kanao, 1995). For example, a record section after band-pass filtered at 8-15 Hz using a normal-moveout velocity of 6.3 km/s is shown in Fig. 13. This record section will give the structure approximately 150 km inland from the coast. The amplitudes at distant stations from SHOT 19 were likely to be over-magnified, because the time span was elongated by a normal-moveout correction. Nevertheless, we can detect enhanced reflected waves in the distance range of 80 - 200 km at 8 - 16 s two-way travel time (TWT), showing clear reflection of the crust from the late-Preterozoic to Paleozoic ages. The above composite seismograms (Fig. 13) show several interesting features. As a whole, large phases were identified in the range from 8 to 17 s TWT. Clear phases around 12 s TWT (e.g., 07 and 08 stations) can be considered as reflected from the top of the lower crust (6.8-6.9 km/s of *P*-wave velocity) of about 36 km depth, while those in the range of 8-15 s TWT at 09-15 stations indicate the existence of the reflective lower crust in the corresponding depth of 24-45 km. Since the appearance of large phases is limited within a certain time range, the reflective lower crust is limited within a certain depth range. The large amplitudes appear faster but disappear later towards inland. Therefore, TWT from the coastal area has a larger value than that from the inland area, and the corresponding reflected layer becomes thicker toward inland area. The schematic interpretation of the reflected layers is shown in the lower part of Fig. 14, together with the *P*-wave velocity model by Ikami et al. (1984), where typical reflective layers are shown by dashed lines.

5.2. Modeling of reflective layers

The reflective layers indicated in *5.1* correlate to the velocity zone from the lower crust to the uppermost mantle in the near backazimuth groups of 50°-100° and 120°-160°. This evidence indicates that the crustal heterogeneity is mainly correlated with the azimuthal change of the depth for reflective layers. Sandmeier and Wenzel (1990) also tried to detect the lower crustal reflectivity in the Black forest region, Germany, by use of the reflectivity method (Fuchs and Müller, 1971). They also found strong reflectivity with laminated velocity layers in the lower crustal depth with averaged thickness of 120 m. The difference in observed patterns of reflectivity is considered to be correlated with the tectonic history of the crust. Forward simulations were conducted to produce the synthetic receiver functions with a laminated lower crustal model for the neighboring backazimuth in 50°-100° to Mizuho routes. In the simulations, the velocity model by receiver function inversion was adopted as the initial model. The depth range of laminated layers was restricted within 23-34 km (Fig. 15a). We can produce the large amplitudes on later phases around 10-16 s in the receiver functions by assuming velocity laminated zones with 1.0 km thickness in the lower crustal depth (Fig. 15b). These later phases cannot be enhanced enough in the synthetic receiver function computed from the final model of the inversion. We can imply the existence of the velocity laminated zones in the lower crustal depth from the large later phases in the receiver functions. There is a possibility that the number of delay time peaks of the strong amplitudes in Fig. 7 does not represent the actual thickness of laminated layers corresponding to the frequency range higher than 1 Hz.

6. Tectonic interpretation

6.1. Regional crustal evolution

As discussed in the previous chapters, the crustal structure in LHB has some lateral and vertical variations. They are considered to be related to the past regional tectonics, such as the metamorphism in the late-Proterozoic to Paleozoic ages (e.g., Hiroi et al., 1991; Motoyoshi et al., 1989). The last break-up of Gondwana, as in the Antarctica/Australia-India rifting (e.g., Anderson, 1994; Storey, 1995; Hill, 1991), might have created crustal heterogeneity. From the crustal evolution viewpoint, LHB was under compressive stress perpendicular to the thermal axis in the NNW-SSE direction in the last metamorphism age of 500 Ma (Fig. 16). Ishikawa et al. (1994) interpreted the Rundvågshetta region as the highest metamorphic grade area. The fabrics of granulites imply regional ductile deformation during peak metamorphism with the formation of a WNW-ESE subhorizontal mineral lineation, showing development of high-strain structures. Subsequent uplifting of uppermost mantle minerals, such as gabbro, into the crust within the condition of the extensional stress may have followed at the last break up of 150 Ma. The seafloor spreading direction by magnetic anomalies and fracture zone trends south of 63°S at this age are WNW-ESE and NNE-SSW, respectively (Nogi et al., 1992).

The azimuthal differences of the crustal structure by receiver functions between the continental and bay areas may have been influenced by different tectonic history under compressional or extentional stresses. From petrological studies, the continental area is believed to be composed of granulite facies and metamorphic grade increases toward the SW direction (Hiroi et al., 1991; Motoyoshi et al., 1989). The strong velocity variations with depth in the continental backazimuths may be explained by compressional stress during the past metamorphism. The low velocity layers may be composed of felsic rocks in the granulite and amphibolite facies. On the other hand, the bay backazimuths are mostly characterized by gradual velocity increase with depth. The smoothed and gradual increasing crustal velocity patterns together with the broad transitional Moho may be related to the extensional stress patterns at the break-up of Gondwana.

The origin of lower crustal reflectivity is considered from both geologic and geophysical data to have multi-genetic features such as igneous intrusions, lithologic and metamorphic layering, mylonite zones, anastromosing shear zones, seismic anisotropy and fluid layers (e.g., Hyndman and Shearer, 1989; Smithson and Johnson, 1989; Warner, 1990). Although one cause of lower crustal reflectivity is multi-genetic features, the metamorphic layering in the past regional tectonics

is the principal cause in LHB. Strong reflectivity may be expected from deep crust characterized by layered sequences of mafic and felsic rocks (Goff et al., 1994). Moreover, it is also created where mafic rocks are interlayered with upper amphibolite and lower granulite facies metapelites but diminishes when mafic rocks are interlayered with high-grade metapelites (Burke and Fountain, 1990; Holliger et al., 1993). In some regions, the above "primary" causes were enhanced by ductile stretching during the tectonic extensional process. The predominant reflected layers in the lower crust, in particular, are found in the thin-skinned tectonic areas. The reflective lower crust on the Mizuho Plateau may have also been enhanced under the extensional conditions of the last break-up of Gondwana.

Deepening of the lower crustal reflectivity and Moho from Bouguer gravity anomalies along the Mizuho routes may be expected in the typical continental margin area. These dipping crustal structures toward the inland area may also have been affected by the tectonic stresses. There is another possibility that the dipping lower crustal reflectivity on the Mizuho Plateau might be one case of Seaward Dipping Reflector Sequences (SDRS) (Trehu and Wheeler, 1987; Fuis et al., 1986) in the continental margin area of the past Gondwana super-continent. SDRS are observed in the tentative regions of 'Non-volcanic rifting margin' under the tectonically extentional stress between hot-spot areas, such as the Marion - Kerguelen sea plateau. SDRS are considered to belong in the large igneous provinces (LIPs), which were produced by penetration of the athenosphere into the thinning lithosphere during the extensional process when the continental break-up occurred (Anderson, 1994). However, the dipping of the reflective layers on the Mizuho Plateau is in the opposite direction, so the possibility of SDRS is not reliable in LHB.

6.2. Linking velocity to lithology

Harley and Hensen (1990) interpreted the cross-sectional relationship of the Napier Complex, the Rayner Complex and LHC as shown in Fig. 17. Late-Proterozoic structures are interpreted to have been caused by initial uplift and exhumation of the Napier Complex. Cambrian and perhaps more recent faultings are believed to have resulted in sufficient thickening to cause later exposure through erosion, and slightly dipping lamination of the three distinct facies (amphibolite,

transitional and granulite) of LHC along the NE-SW direction. The crustal velocity models of the receiver function inversion in the continental area correspond to two petrological regions of the granulite facies in the 120°-160° backazimuths and of the amphibolite-granulite transitional zone in backazimuths of 50°-100°. There is a small difference, however, in the velocities between amphibolite and mafic granulite facies rocks (Rudnick and Fountain, 1995). Compressional wave velocity generally decreases with increasing SiO_2 for high-grade metamorphic rocks (Fountain et al., 1990). This implies that the crustal velocity models are related to the increase of metamorphic grade along the NE-SW direction.

The seismic velocity structures of the continental crust and the composition as a function of depth by inferring high-pressure laboratory measurements were summarized by Christensen and Mooney (1995). Fig. 18 shows the shear velocity models by receiver function inversion in the two backazimuth groups (modified by Figs. 9a, 10a with error bars), average velocity model for shields and platforms compared to averaged laboratory measured velocities in metamorphic rocks (modified by Cristensen and Mooney, 1995). Rock velocities are measured to pressure of 1 GPa, which is equivalent to crustal depth of 35 km. Velocities versus depth for the laboratory are shown as the low geotherm model, because the surface heat flow in LHB is about 42 mW/m^2 (Pollack and Chapman, 1977). In order to produce Fig. 18, compressional wave velocities were converted to shear velocities by assuming the common Vp/Vs ratio of 1.73 for all rock types.

In the granulite facies backazimuths of 120°-160°, high velocity zones are recognized in 2-10 km depth, which are considered to be composed of the contamination of felsic and mafic rocks. Low velocity zones in the middle crustal depth of 10-30 km are likely to be composed of felsic granulite. Lower crustal depth with high velocity is mainly characterized by the mafic rocks such as mafic garnet granulite. On the contrary, in the amphibolite-granulite transitional zone backazimuths of 50°-100°, low velocity zones in the upper crustal depth and high velocity zones in the middle crustal depth are recognized; the latter is consistent with the average velocity model for shields. The higher velocities in the middle and lower crust than those in the granulite facies backazimuths may be originated from large volume percentages of mafic rocks such as amphibolite, anorthositic granulite, mafic granulite and/or mafic garnet granulite. As for the uppermost mantle in both

backazimuth groups, mafic eclogite facies and the other ultramafic rocks are the main compositions in order to originate the mantle velocity.

Cristensen and Mooney (1995) modeled the petrology of the average continental crust based on a selection of rock assemblages which are commonly observed in exposures of crustal section, that is, the association of granitic gneiss, tonalitic gneiss, amphibolite, mafic granulite and mafic garnet granulite. The weighted averaged crustal velocity-depth curve from the above metamorphic rocks is simulated in order to fit the observed average crustal model. The initiation of major reflectors at midcrustal depths originates from the large contrasts in acoustic impedance of amphibolite with granitic gneiss and tonalitic gneiss. In the deeper crust, garnet-rich layers, with high densities and velocities, are likely to be significant reflectors. This model will be applied to LHB as a first approximation so as to explain the high velocity zones in the lower crustal depth and crustal reflective layers as seen in *5.1*. It is important to assume the gradual increase of volume percentages of mafic rocks and the lamination of several metamorphic rocks in the lower crust. However, the discontinuities between two distinct facies in the dipping lamination as illustrated in Fig. 17 cannot be exactly identified by the presently available data.

7. Discussion

7.1. Crustal thickness from Bouguer gravity anomalies

The reflection pattern in the lower crust of the Mizuho Plateau is shown to be related to the gravity anomalies, particularly to the Bouguer anomalies. Gravity surveys on the Mizuho Plateau have been carried out along several traverse routes since 1961 (e.g., Yanai and Kakinuma, 1971; Yoshida and Yoshimura, 1971; Abe, 1975; Nagao and Kaminuma, 1984, 1988; Ageta et al., 1987; Nishio et al., 1988). Nagao et al. (1991) and Kudo and Nagao (1994) compiled these gravity data and presented three-dimensional contour maps of gravity anomalies. In 1992, the gravity measurements were also conducted along the traverse routes to Dome-F (77.4°S, 39.6°E), 900 km

inland from the Prince Olav Coast (Kamiyama et al., 1994). In order to compare with the crustal velocity structures by seismological evidence, free-air and Bouguer gravity anomalies along the Mizuho routes (Shimizu et al., 1972; Yoshida and Yoshimura, 1972; Abe, 1975; Kamiyama et al., 1994) are plotted on the upper part of Fig. 14. The thickening reflective layers are shown to have a correlation with the decreasing Bouguer gravity anomalies along the routes from the Soya Coast until 150 km inland; which must reflect density contrast corresponding to the Conrad and Moho depths.

The crustal density model along the Mizuho routes was obtained by fitting the calculated Bouguer anomalies to the observed ones (Ito and Ikami, 1986) with an application of the layered density model (Talwani et al., 1959). When we extend this crustal density model to Dome-F, toward the southern area around Mizuho Station (Kanao et al., 1994), the Moho depth will increase from 40 km at the Soya Coast to about 48 km at Dome-F. For reference, Nagao and Kaminuma (1984) showed similar difference of the Moho depth of 4 km increase in the Yamato Mountains as compared with LHB from the Bouguer anomalies. The dipping Moho toward the inland area is schematically indicated in Fig. 14 as 'the bottom of the reflective layers'. These deep dipping reflective layers corresponding to the lower crust might indicate that the ancient structure existed in Precambrian time, and persisted through time under the long-term thermal and tectonic stability.

When we assume the dipping reflective crustal layers, the amplitude and arrival times as a function of backazimuth and hypocentral distance will be affected in the receiver function analysis (Cassidy, 1992). The tight stacking backazimuth range and limited hypocentral distance range may avoid amplitude attenuation of *Ps* phases and energy scattering. In this study, however, such stacking bounds were constrained to make the observed receiver functions then the velocity models in the distinct backazimuths can be reliable.

7.2. Heat flow, free-air gravity anomalies and effect of ice sheet

The relationship between the depth to the top of the lower crustal reflective layers and the surface heat flow is pointed out as the slightly decreasing linearity in the different geological terranes (Klemperers et al., 1987). The low heat flow of 42 mW/m^2 around LHB (Pollack and

Chapman, 1977) corresponds to the deep and thick reflective layers beneath 25 km depth, which correlates well with the depth from about 24 to 45 km by reflection analysis as shown in *5.1*. If the above correlation maintaines over geological time-scales, the lower crustal reflectivity may has been diminished through the crust in response to the changes of crustal temperature. The evidence of deep reflection layers is also well associated with the structure that formed during the late-Preterozoic to Paleozoic metamorphic ages in LHB.

The free-air gravity anomalies in LHB combined by both the satellite altimeter data and the surface gravity data (Fukuda, 1990) indicate negative anomalies within the bay, which coincides with the high velocity area of the upper crust in the bay backazimuths of 210°-360° from the receiver function inversion. On the other hand, the positive gravity anomalies are located around the southern part in LHB from the Shirase Glacier, Yamato Mountains and on the Mizuho Plateau; they have correlation with the low velocity area within the upper crust of the continental backazimuths. The positive gravity anomalies are in the northern part of LHB, which is considered to be the continental margin of the last break-up of Gondwana.

The effect of Antarctic ice sheet might affect the present investigations using short period seismic waveforms. The surface layer in the initial model in the receiver function inversion should be taken into consideration on the basis of the actual ice sheet velocity model. The phase velocities of fundamental mode Rayleigh waves in East Antarctica can be affected by the existence of the ice sheet for waves having periods of some tens of seconds (Knopoff and Vane, 1979). Waves of period more than a few hundred seconds, in particular tidal waves, can also be affected by the ice sheet. Tidal gravity observations were started at SYO from 1992 (e.g., Kanao and Sato, 1993) using a LaCoste&Romberg gravity meter with an electrostatic feedback amplifier. The obtained tidal (δ) factors after the correction of oceanic tidal loading effects were 1.177 (O1), 1.149 (K1), 1.270 (M2), and 1.274 (S2), respectively. The diurnal δ factors agree with those predicted by Melchior and De Becker (1983). In contrast, the semidiurnal δ factors are 10 per cent larger than the theoretical values given by Wahr (1981). Tidal analyses resulted in a gravity admittance of -0.291 μGal/hPa for the air pressure change and 0.575 μGal/°C for the temperature change, respectively. The smaller magnitude of the pressure admittance compared with the typical value of

-0.35 μGal/hPa for a normal crust may be explained by the loading deformation of the ice sheet under the air mass.

7.3. Crustal anisotropy

In order to obtain the shear wave anisotropy of the crust, splitting analysis was applied to the observed receiver functions. Moho *Ps* phases in the receiver functions will effectively produce the crustal anisotropy (e.g., McNamara and Owens, 1993). Actually, the strong amplitudes of Moho *Ps* phases are recognized around 4-5 s after *P*-arrival in all the backazimuths (Fig. 7). The splitting analysis of Moho *Ps* phases was applied to the 12 receiver functions with clear amplitudes in the transverse component, followed by the three solutions within allowable error estimation (Fig. 19; Kanao et al., 1996). The obtained crustal anisotropy beneath SYO is quantified by the averaged fastest direction in N133°E and time difference of polarized waves as 0.5 s. The crustal anisotropy may mainly have been originated from the metamorphic rocks in the crustal composition. High-grade granulite facies observed in the surface outcrops around SYO are characterized by relatively low in anisotropy rather than from low grade metamorphic rocks and mantle compositions (Christensen and Mooney, 1995). The observed crustal anisotropy, therefore, may be produced by the high-grade mafic compositions, such as garnet granulite and paragranulite and/or medium grade amphibolite facies rocks within the crust. It is also reported that the 5 per cent anisotropy of *P*-wave velocity exist in the granulite facies rocks of the Arunta block, central Australia (Greenhalgh et al., 1990).

The splitting analyses of the *SKS* phases were also done by using the broadband data at SYO (Kubo et al., 1995). The fastest direction and the arrival time difference between fast and slow polarized waves were estimated as N49°E and 0.7 s, respectively (see Fig. 19). Since this fastest direction for *SKS* phases is not coincident with that in N120°E from the present mantle flow by the HS2-NUVEL1 model (Gripp and Gordon, 1990), the anisotropy for shear waves of the region concerned may still preserve past tectonic features. The NNW-SSE direction of the maximum thermal axis of the last metamorphism at 500 Ma from petrological studies (Motoyoshi et al., 1989; Hiroi et al., 1991) is perpendicular to the fastest *SKS* splitting direction, and parallel to that from

Moho *Ps* phases. This may indicate that the paleo athenospheric flow of the last metamorphism must have been a primary effect producing the polarization anomalies of *SKS* phases. The crustal fast splitting direction of N133°E, on the contrary, might have been oriented by both the past regional metamorphism and next stage of the extensional process. Anisotropy obtained by *SKS* phases incorporated both crust and upper mantle effects and it is difficult to distinguish them. Since the fast splitting directions of Moho *Ps* and *SKS* phases are almost perpendicular to each other, the actual anisotropy only in the upper mantle may presumably be larger than the observed ones.

It is considered that crustal anisotropy has some relation to the lateral heterogeneity by the azumithual variation of the shear velocity models by receiver function inversion. Actually, the crustal velocities in the backazimuths of 120°-160° and 300°-310° have higher crustal velocities than in the other backazimuths. The difference in velocity is related to the phase arrival-time, but is not affected by the shear wave anisotropy.

7.4. Further investigations

Since the crustal velocity models for *P*- and *S*- waves have been obtained in LHB by both the refraction experiments and receiver function inversion analyses, the elastic parameter, the *Vp/Vs* ratio, and its depth-distribution should be determined in the late-Proterozoic to Paleozoic crust in East Antarctica. The crustal *Vp/Vs* for all continents except Antarctica was estimated from the ratio of differential times as *(Ps-P)/(PpPms-Ps)* (Zandt and Ammon, 1995). The presence of a mafic lower crust beneath cratons has been clarified but the difference between Archean and Proterozoic crust has not yet been obtained. Therefore, mapping of *Vp/Vs* on the Antarctic continent by using the receiver function must be a fascinating study for the near future.

Early seismic reflection profiles in the Precambrian crust indicated a generally structureless lower crust, however, recent reflection studies have revealed pronounced structural features of steeply dipping zones of reflections deeper than 15 km, from the lower crust and Moho (e.g., Smithson and Johnson, 1989; Ross et al., 1995). These observed Precambrian structures imply the existence of ancient tectonics, persisting with long-term thermal and tectonic stability. Since

most Precambrian data collected to date are from Preterozoic terranes, the deep reflection profiling of Archean crust remains a scientific frontier.

Comparison of crustal structures of different geological terranes such as the Napier, the Rayner and the Yamato-Belgica Complexes (Shiraishi et al., 1992, 1994; Harley and Hensen, 1990) is very interesting as it reveals the transitional structures among several ancient orogens of continental crust from Archean to Phanerozoic ages. In order to compare the structural difference between the Complexes, the reflection surveys in the long profiles are necessary in addition to a dense network of broadband seismometers. The reflection sections can be compared as for the velocity structures derived by the receiver function inversion. The reological approaches give also useful information to interpret crustal reflectivity and heterogeneity.

Moreover, compared with other tectonic regions such as island arcs, continental collision and/or rift regions, extension fields, and continental margins, it is useful to construct fine crustal models by several seismological approaches. The spacing of observation stations, however, is too sparse to provide a clear image of the crustal structures including reflective patterns of the lower crust. At present, analyses of available broadband data in Antarctica should be promoted.

8. Conclusions

In this paper, the crustal structure for shear waves in LHB is investigated by making use of the presently available seismological waveform data, such as those from local and teleseismic earthquakes and refraction data, to obtain insight into a tectonic interpretation to the evolution of LHB. The past regional tectonics, such as a metamorphism in the late-Proterozoic to Paleozoic ages is considered to have a relationship. The obtained results are summarized as follows:

1) LHB was under compressive stress perpendicular to the thermal axis in the NNW-SSE direction in the last metamorphism age of 500 Ma as the Cambrian orogenic belt. This regional metamorphism might have created crustal heterogeneity. The large amplitudes

around 4-5 s after *P*-arrivals are significant in the observed receiver functions; they are Moho *Ps* phases at depth around 40 km. Lateral heterogeneity of the crust is confirmed by the receiver function analyses of the four backazimuth groups. In the continental backazimuths in 50°-160°, crustal velocity variations are large and the Moho is rather sharp at 36-38 km depth, while it is smooth and transitional in the bay backazimuths in 210°-360°.

As for the continental backazimuths of 120°-160° corresponding to significant granulite facies, the velocity model has larger variations with high velocity zones in the upper crustal depth than that for the transitional and amphibolite facies backazimuths of 50°-100°. The gradual increase of complexity in the crustal velocity models in the clockwise direction implies increasing metamorphic grade along the NE-SW direction in LHB. High velocity zones in the upper crust of granulite facies and in the middle crust of granulite-amphibolite transitional facies backazimuths may be consistent with the velocity of the mafic granulite facies found from laboratory data.

Crustal reflectivity detected by re-analysis of refraction data on the Mizuho Plateau is explained by the crustal thickening in the past metamorphism in LHB and a subsequent metamorphic layering, such as the layered sequences of mafic and felsic rocks. The depth of reflective layers is within 24-45 km, which is related to the Bouguer gravity anomalies on the traverse routes. Crustal anisotropy was quantified by the averaged fastest direction of N133°E and time difference of polarized waves of 0.4 s by splitting analysis of Moho *Ps* phases. The fast splitting direction in the crust is perpendicular to that in the upper mantle as found by the analysis of *SKS* phases. The paleo athenospheric flow of the last metamorphism must have been a primary effect producing the polarization anomalies of shear waves.

2) At 150 Ma, there was the break-up of Gondwana super-continent in relation to the Antarctica/Australia-India rifting when LHB was under the condition of extentional stress in the NW-SE direction, which is perpendicular to that in the regional metamorphism. Lateral heterogeneity of the crust confirmed by the receiver function analyses might have been associated with this last break-up. The feature as the continental margin area in East

Antarctica is also indicated by the Moho depth estimated from the Bouguer anomalies with dipping from 40 km in the coastal area to 48 km beneath Dome-F, 900 km inland.

Lower crustal reflectivity formed in the regional metamorphism as the above "primary" causes were enhanced by ductile stretching during the tectonic extensional process of Gondwana break-up. Otherwise, the reflective layers were accreted by uplifting of the mantle material and/or underplating.

3) LHB has the above tectonics without any special thermal activities after the regional metamorphism at 500 Ma. The present crust has been experienced the cooling down and the up-lifting about 15 km. This old history of crustal evolution is supported by the evidence of thick lithosphere with low surface heat flow about 40 mW/m^2 and the deep reflective layers. Crustal attenuation model for shear waves is determined by the coda-Q inversion method in the frequency range of 1-24 Hz for local earthquakes. The obtained model is characterized by weak attenuation and strong frequency dependence on Q_S, in contrast to other active tectonic regions. The thick homogeneous lithosphere is characteristic of the stable metamorphic shield region in East Antarctica.

Acknowledgments

The author wishes to thank the Syowa wintering members, led by M. Fukuchi, for their generous support and encouragement. The author expresses his sincere thanks to Profs. H. Watanabe, K. Ito, K. Oike, M. Shimada, J. Akamatsu, K. Hirahara and M. Ando in the Disaster Prevention Research Institute, Kyoto University for their valuable advice and discussions for improving the manuscript. He would also like to thank Profs. K. Kaminuma, K. Shibuya, K. Shiraishi and Y. Motoyoshi in the National Institute of Polar Research for their valuable advice and discussions concerning regional geophysical and geological interpretations. He also thanks to Drs. T. Shibutani, M. Kosuga, Y. Nogi and A. Kubo for their grateful support including the use of inversion programs, data acquisitions and discussions. The author was partially supported by Grants 40233845 from the Ministry of Education, Science and Culture of Japan during the latter stages of this study. Data processing was done on UNIX workstations at the Earth Science Division, National Institute of Polar Research.

References

Abe, Y., 1975. Gravity data. JARE Data Rep., 28 (Glaciology 3): 114-119.

Ageta, Y., Kikuchi, T., Kamiyama, K. and Okuhira, F., 1987. Glaciological research program in East Queen Maud Land, East Antarctica; Part 5. JARE Data Rep., 125 (Glacio. 14): 71.

Akamatsu, J., 1980. Attenuation property of coda parts of seismic waves from local earthquakes. Bull. Disas. Prev. Res. Inst., Kyoto Univ., 30: 1-16.

Akamatsu, J., Ichikawa, N. and Kaminuma, K., 1989. Seismic observation with local telemetry network around Syowa Station, East Antarctica. Proc. NIPR Symp. Antarct. Geosci., 3: 1-12.

Akamatsu, J., Ichikawa, N. and Kaminuma, K., 1990. Seismic observation with local telemetry network around Syowa Station, East Antarctica (2). Proc. NIPR Symp. Antarct. Geosci., 4: 90-99.

Akamatsu, J., 1991. Coda attenuation in the Lützow-Holm Bay region, East Antarctica. Phys. Earth Planet. Inter., 67: 65-75.

Akamatsu, J., Kaku, H. and Kanao, M., 1995. Coda Q of local earthquakes observed on the southeast Tibetan Plateau -Comparison with Lützow-Holm Bay region, East Antarctica-. Proc. NIPR Symp. Antarct. Geosci., 8: 15-24.

Aki, K., 1969. Analysis of the seismic coda of local earthquakes as scattered waves. J. Geophys. Res., 74: 615-631.

Aki, K. and Chouet, B., 1975. Origin of coda waves; source, attenuation and scattering effects. J. Geophys. Res., 80: 3322-3342.

Anderson, D. L., 1994. Superplumes or supercontinents ?. Geology, 22: 39-42.

Ammon, C. J., Randall, G. E. and Zandt, G., 1990. On Nonuniqueness of Receiver Function Inversion. J. Geophys. Res., 95: 15303-15318.

BABEL Working Group, 1990. Evidence for early Proterozoic platetectonics from seismic reflection profiles in the Baltic shield. Nature, 348: 34-38.

Bentley, C. R., 1983. Crustal structure of Antarctica from geophysical evidence. A review. In: R. L. Oliver, P. R. James and J. B. Jago (Editors), Antarctic Earth Science, Australia Acad. Science, Camberra, 491-497.

Black, L., Harley, S. L., Sun, S. S. and McCulloch, M. T., 1987. The Rayner complex of East Antarctica: complex isotopic systematics within a Proterozoic mobile belt. Jour. Metamor. Geol., 5: 1-26.

Burke, M. M. and Fountain, D. M., 1990. Seismic anisotropy of metapelites from the Ivrea-Verbano zone and Serie dei Laghi (northern Italy). Phys. Earth Planet. Inter., 78: 301-317.

Cassidy, J. F., 1992. Numerical experiments in broadband receiver function analysis. Bull. Seism. Soc. Am., 82: 1453-1474.

Christensen, N. I. and Mooney, W. D., 1995. Seismic velocity structure and composition of the continental crust: A global view. J. Geophys. Res., 100: 9761-9788.

Correig, A. M., Mitchell, B. J. and Ortiz, R., 1990. Seismicity and coda Q values in the eastern Pyrenees: first results from the La Cerdanya seismic network. Pure Appl. Geophys., 132: 311-329.

Dewart, G. M. and Toksöz, M. N., 1965. Crustal structure in East Antarctica from surface wave dispersion. Geophys. J. R. Astron. Soc., 10: 127-139.

Eck, V. T., 1988. Attenuation of coda waves in the Dead Sea region. Bull. Seism. Soc. Am., 78: 770-779.

Ellis, D. J., 1983. The Napier and Rayner Complexes of Enderby Land, Antarctica - contrasting styles of metamorphism and tectonism. In: R. L. Oliver, P. R. James and J. B. Jago (Editors), Antarctic Earth Science: Canberra, Austral. Acad. Sci., 20-24.

Evison, F. F., Ingham, C. E., Orr, R. H. and le Fort, J. H., 1960. Thickness of the Earth's crust in Antarctica and the surrounding oceans. Geophys. J. R. Astron. Soc., 3: 289-306.

Fountain, D. M., Salisbury, M. H. and Percival, J., 1990. Seismic structure of the continental crust based on rock velocity measurements from the Kapuskasing uplift. J. Geophys. Res., 95: 1167-1186.

Fuchs, K. and Müller, G., 1971. Computation of synthetic seismograms with the reflectivity method and comparison with observations. Geophys. J. R. Astron. Soc., 23: 417-433.

Fuis, G. S., Walter, A. W., Mooney, W. D. and McCarthy, J., 1986. Crustal structure of the Salton Trough, western Mojave Desert, and Colorado Desert, from seismic refraction. Geol. Soc. Am. Abstr. Programs, 18:107-108.

Fukuda, Y., 1990. Precise determination of local gravity field both the satellite altimeter data and the surface gravity data. Bull. Ocean Res. Inst., 28: 1-133.

Goff, J. A., Holliger, K. and Levander, A., 1994. Modal fields: A new method for characterization of random velocity heterogeneity. Geophys. Res. Lett., 21: 493-496.

Goleby, B. R., Kennett, B. L., Wright, C., Shaw, R. D. and Lambeck, K., 1990. Seismic reflection profiling in the Proterozoic Arunta Block, central Australia: processing for testing models of tectonic evolution. In: J. H. Leven, D. M. Finlayson, C. Wright, J. C. Dooley and B. L. N. Kennett (Editors), Seismic Probing of Continents and their Margins, Tectonophysics, 173: 257-268.

Green, A., Cannon, W., Milkereit, B., Hunchinson, D., Davidson, A., Behrendt, J., Spencer, C., Lee, M., Morel-a-Hussier, P. and Agena, W., 1989. A "Gilmpce" of the deep crust beneath the Great Lakes. In: R. F. Mereu, S. Mueller and D. M. Fountain (Editors), Properties and Processes of Earth's Lower Crust, Am. Geophys. Union, Geophys. Monogr., 51: 65-80.

Greenhalgh, S. A., Wright, C., Goleby, B. and Soleman, S., 1990. Seismic anisotropy in granulite facies rocks of the Arunta block, central Australia. Geophys. Res. Lett., 17: 1513-1516.

Gripp, A. E. and Gordon, R., 1990. Current plate velocities relative to the hot spots incorporating the NUVEL-1 global plate motion model. Geophys. Res. Lett., 7: 1109-1112.

Harley, S. and Hensen, B. J., 1990. Archean and Proterozoic high-grade terranes of East Antarctica (40°-80°E): a case study of diversity in granulite facies metamophism. In: J. R. Ashworth and M. Brown (Editors), High Temperature Metamorphism and Crustal Anatexis, London, Unwin-Hyman, 320-370.

Hill, R. I., 1991. Starting plumes and continental break-up. Earth Planet. Sci. Lett., 104: 398-416.

Hiroi, Y., Shiraishi, K. and Motoyoshi, Y., 1991. Late Proterozoic paired metamorphic complexes in East Antarctica, with special reference to the tectonic significance of ultramafic

rocks. In: M. R. A. Thomson, J. A. Crame and J. W. Thomson (Editors), Geological Evolution of Antarctica, Cambridge, Cambridge Univ. Press, 83-87.

Holliger, K., Levander, A. R. and Goff, J. A., 1993. Stochastic modeling of the reflective lower crust: Petrophysical and geological evidence from the Ivrea zone (northern Italy). J. Geophys. Res., 98: 11967-11980.

Hyndman, R. D. and Shearer, P. M., 1989. Water in the lower continental crust: modelling magnetotelluric and seismic reflection results. Geophys. J., 98: 343-365.

Ikami, A., Ito, K., Shibuya, K. and Kaminuma, K., 1984. Deep crustal structure along the profile between Syowa and Mizuho Stations, East Antarctica. Mem. Nat. Inst. Polar Res., Ser. C (Earth Sci.), 15: 19-28.

Ishikawa, M., Motoyoshi, Y. Fraser, G. L. and Kawasaki, T., 1994. Structural evolution of Rundvågshetta region, Lützow-Holm Bay, East Antarctica. Proc. NIPR Symp. Antarct. Geosci., 7: 69-89.

Ito, K. and Ikami, A., 1984. Upper crustal structure of the Prince Olav Coast, East Antarctica. Mem. Nat. Inst. Polar Res., Series C (Earth Sci.), 15: 13-18.

Ito, K. and Ikami, A., 1986. Crustal structure of the Mizuho Plateau, East Antarctica from geophysical data. Jour. Geod., 6: 285-296.

Ito, K. and Kanao, M., 1995. Detection of reflected waves from the lower crust on the Mizuho Plateau, East Antarctica. Nankyoku Shiryo (Antarct. Rec.), 39: 233-242.

Jin, A., Cao, T. and Aki, K., 1985. Regional change of coda Q in the oceanic lithosphere. J. Geophys. Res., 90: 8651-8659.

Kadmina, I. N., Kurinin, R. G., Masolov, V. N. and Grikurov, G. E., 1983. Antarctic crustal structure from geophysical evidence; A review. In: R. L. Oliver, P. R. James and J. B. Jago (Editors), Antarctic Earth Science, Australia Acad. Science, Camberra, 498-502.

Kaminuma, K., Eto, T. and Yoshida, M., 1968. Seismological observation at Syowa Station, Antarctica. Nankyoku Shiryo (Antarct. Rec.), 33: 65-70.

Kaminuma, K., Segawa, J., Fukuda, Y., Ito, K., Nagao, T., Ikami, A., Funaki, M., Shiraishi, K., Hiroi, Y., Moriwaki, K. and Yoshida, Y., 1991. Antarctic geoscience transect QML-1A and QML-1B. Special map series of Nation. Inst. Polar Res., 5.

Kamiyama, K., Furukawa, T., Maeno, H., Kishi, T. and Kanao, M., 1994. Glaciological Data Collected by the 33rd Japanese Antarctic Research Expedition in 1992. JARE Data Rep., 194 (Glaciology 21): 1-67.

Kanao, M. and Ito, K., 1990. Attenuation property of coda waves in the middle and northern parts of Kinki district. Zisin (J. Seism. Soc. Jpn.), Ser. 2, 43: 311-320.

Kanao, M. and Ito, K., 1991. Attenuation of S waves and coda waves in the inner zone of southwestern Japan. Bull. Disas. Prev. Res. Inst., Kyoto Univ., 41: 87-107.

Kanao, M. and Ito, K., 1992. Attenuation of coda waves in the source area of the 1990 July Luzon Earthquake, Philippines. Bull. Disas. Prev. Res. Inst., Kyoto Univ., 42: 31-51.

Kanao, M. and Sato, T., 1993. Observation of the Earth tide and free oscillation of the Earth by LaCoste & Romberg gravity meter at Syowa Station, East Antarctica. Proc.12th International Symposium on Earth Tides, Beijing, 571-580.

Kanao, M. and Kaminuma, K., 1994a. Performance test of STS-seismograph in low temperature. Nankyoku Shiryo (Antarct. Rec.), 38: 199-231.

Kanao, M. and Kaminuma, K., 1994b. Broadband and wide dynamic-range seismic observations with an STS-seismograph at Syowa Station, East Antarctica. Proc. NIPR Symp. Antarct. Geosci., 7: 1-13.

Kanao, M., Kamiyama, K. and Ito, K., 1994. Crustal density structure of the Mizuho Plateau, East Anatrctica from gravity survey in 1992. Proc. NIPR Symp. Antarct. Geosci., 7: 23-36.

Kanao, M. and Akamatsu, J., 1995. Shear wave Q structure for lithosphere in the Lützow-Holm Bay region, East Antarctica. Proc. NIPR Symp. Antarct. Geosci., 8: 1-14.

Kanao, M. and Kaminuma, K., 1995. Detection capability of earthquakes recorded at Syowa Station, Antarctica, from 1987 to 1993. Nankyoku Shiryo (Antarct. Rec.), 39: 156-169.

Kanao, M., Kaminuma, K., Shibuya, K. and Nogi, Y., 1995. Transfer, archives and public use of digital data for solid earth geophysics at Syowa Station, Antarctica by computer network. Nankyoku Shiryo (Antarct. Rec.), 39: 303-320.

Kanao, M., Kubo, A., Hiramatsu, Y. and Shibutani, T., 1996. Crustal heterogeneity and anisotropy for shear waves in the Lützow-Holm Bay region, East Antarctica by broadband

teleseismic waveforms, (submitted to) Proc. VII Inter. Symp. Antarct. Earth Sci., Siena, Italy.

Kind, R., Kosarev, G. L. and Petersen, N. V., 1995. Receiver functions at the stations of the German Regional Seismic Network (GRSN). Geophys. J. Int., 121: 191-202.

Klemperers, S. L. and the BIRPS Group, 1987. Reflectivity of the crystalline crust: hypotheses and tests. Geophys. J. Roy. Astr. Soc., 89: 217-222.

Knopoff, L. and Vane, G., 1979. Age of East Antarctica from surface wave dispersion. Pageoph, 117: 806-815.

Kosuga, M., 1992. Dependence of coda Q on frequency and lapse time in the western Nagano region, central Japan. J. Phys. Earth, 40: 421-445.

Kovach, R. L. and Press, F., 1961. Surface wave dispersion and crustal strucutre in Antarctica and the surrounding oceans. Ann. Geofis., 14: 211-224.

Kubo, A., Hiramatsu, Y., Kanao, M., Ando, M. and Terashima, T., 1995. An analysis of the SKS splitting in Antarctica. Proc. NIPR Symp. Antarct. Geosci., 8: 25-34.

Kudo, T. and Nagao, T., 1994. Re-evaluation of crustal structure and bedrock topography around Mizuho Plateau, Antarctica based on gravity data. Proc. NIPR Symp. Antarct. Geosci., 7: 37-48.

Langston, C. A., 1979. Structure under Mount Rainier, Washington, inferred from teleseismic body waves. J. Geophys. Res., 84: 4749-4762.

Lawson, C. L. and Hanson, R. J., 1974. Solving least squares problems. Chap. 23, Englewood Cliffs, NJ, Prentice-Hall Inc., 158-173.

Lupei, Z., Rongsheng, Z., Wu, F. T., Owens, T. J. and Randall, G. E., 1994. Study on the crust-upper mantle structure of Qinghai-Tibet Plateau by using broadband teleseismic body waveforms. Acta Seismologica Sinica, 37: 259-266.

McNamara, D. E. and Owens, T. J., 1993. Azimuthal Shear Wave Velocity Anisotropy in the Basin and Range Province Using Moho Ps Converted Phases. J. Geophys. Res., 98: 12003-12017.

Melchior, P. and De Becker, M., 1983. A discussion of world-wide measurements of tidal gravity with respect to oceanic interactions, lithosphere heterogeneities, Earth's flattening and inertial forces. Phys. Earth Planet. Inter., 31: 27-53.

Mooney, W. D. and Brocher, T. M., 1987. Coincident seismic reflection/refraction studies of the continental lithosphere: a global review. Rev. Geophys., 25: 723-742.

Motoyoshi, Y., Matsubara, S. and Matsueda, H., 1989. *P-T* evolution of the granulite-facies of the Lützow-Holm Bay region, East Antarctica. In: J. S. Daly, R. A. Cliff and B. W. D. Yardley (Editors), Evolution of Metamorphic Belts, Geological Society Special Publication, 43: 325-329.

Nagao, T. and Kaminuma, K., 1984. Estimation of the crustal and the bedrock topography by the gravitational method around Syowa Station, East Antarctica. Mem. Natl Inst. Polar Res., Special Issue, 33: 1-8.

Nagao, T. and Kaminuma, K., 1988. Gravity survey in the Mizuho Plateau. JARE Data Rep., 132 (Earth Science 4): 1-32.

Nagao, T., Awara, M. and Kaminuma, K., 1991. Three-dimensional topographic and gravity anomaly maps in the vicinity of Mizuho Plateau, East Antarctica. Nankyoku Shiryo (Antarct. Rec.), 35: 56-69.

Nagasaka, K., Kaminuma, K. and Shibuya, K., 1992. Seismological observations by a three-component broadband digital seismograph at Syowa Station, Antarctica. In: Y. Yoshida, K. Kaminuma and K. Shiraishi (Editors), Recent Progress in Antarctic Earth Science, Tokyo, Terra Sci. Publ., 595-601.

Nishigami, K., Iio, Y., Gurbuz, C., Pinar, A., Aybey, N., Ucer, S. B., Honkura, Y. and Isikara, A. M., 1990. Microseismic activity and spatial distribution of coda Q in the westernmost part of the north Anatolian fault zone, Turkey. Bull. Disas. Prev. Res. Inst., Kyoto Univ., 40: 41-56.

Nishio, F., Ohmae, H. and Ishikawa, M., 1988. Bedrock and ice surface profiles in the Shirase Glacier basin determined by the ground-based radio-echo sounding. Bull. Glacier Res., 6: 33-39.

Nogi, Y., Seama, N. and Isezaki, N., 1992. The directions of magnetic anomaly lineations in Enderby Basin, off Antarctica. In: Y. Yoshida, K. Kaminuma and K. Shiraishi (Editors), Recent Progress in Antarctic Earth Science, Tokyo, Terra Sci. Publ., 649-654.

Owens, T. J., Zandt, G. and Taylor, S. R., 1984. Seismic Evidence for an Ancient Rift Beneath the Cumberland Plateau, Tennessee: A Detailed Analysis of Broadband Teleseismic P Waveforms. J. Geophys. Res., 89: 7783-7795.

Owens, T. J. and Zandt, G., 1985. The response of the continental crust-mantle boundary observed on broadband teleseismic receiver functions. J. Geophys. Res. Lett., 12: 705-708.

Owens, T. J., 1987. Crustal Structure of the Adriondacks Determined From Broadband Teleseismic Waveform Modeling. J. Geophys. Res., 92: 6391-6401.

Polet, J. and Anderson, D. L., 1995. Depth extent of cratons as infered from tomographic studies. Geology, 23: 205-208.

Pollack, H. N. and Chapman, D. S., 1977. Mantle heat flow. Earth Planet. Sci. Lett., 34: 174-184.

Pulli, J. J., 1984. Attenuation of coda waves in New England. Bull. Seismol. Soc. Am., 74: 1149-1166.

Ross, G. M., Milkereit, B., Eaton, D., White, D., Kanasewich, E. R. and Burianyk, M. J. A., 1995. Paleoproterozoic collisional orogen benearth the western Canada sedimentary basin imaged by Lithoprobe crustal seismic-reflection data. Geology, 23: 195-199.

Rouland, D. and Roult, G., 1992. Phase Velocity Distribution Beneath Antarctica and Surrounding Oceans, Recent Progress in Antarctic Earth Science. In: Y. Yoshida, K. Kaminuma and K. Shiraishi (Editors), Recent Progress in Antarctic Earth Science, Tokyo, Terra Sci. Publ., 483-487.

Roult, G., Rouland, D. and Montagner, J. P., 1994. Antarctica II: Upper-mantle structure from velocities and anisotropy. Phys. Earth Planet. Inter., 84: 33-57.

Rudnick, R. L. and Fountain, D. M., 1995. Nature and composition of the continental crust: a lower crustal perspective. Rev. Geophys., 33: 267-309.

Sandmeier, K. J. and Wenzel, F., 1990. Lower crustal petrology from wide-angle P- and S-wave measurements in the Black Forest. In: J. H. Leven, D. M. Finlayson, C. Wright, J. C.

Dooley and B. L. N. Kennett (Editors), Seismic Probing of Continents and their Margins. Tectonophysics, 173: 495-505.

Sato, H., 1986. Regional study of coda Q^{-1} in the Kanto-Tokai district, Japan. Zisin (J. Seismol. Soc. Jpn.), 39: 241-249.

Shibutani, T., 1993. A new method of receiver function inversion for investigating S wave velocity structure of the crust and uppermost mantle. Ph. D. thesis, Kyoto University, Kyoto.

Shimizu, H., Naruse, R., Omoto, K. and Yoshimura, A., 1972. Position of stations, surface elevation and thickness of the ice sheet, and snow temperature at 10 m depth in the Mizuho Plateau-West Enderby Land area, East Antarctica, 1969-1971. JARE Data Rep., 17 (Glaciology 1): 12-37.

Shiraishi, K., Hiroi, Y., Ellis, D. J., Fanning, C. M., Motoyoshi, Y. and Nakai, Y., 1992. The first report of a Cambrian orogenic belt in East Antarctica -An ion microprobe study of the Lützow-Holm Complex. In: Y. Yoshida, K. Kaminuma and K. Shiraishi (Editors), Recent Progress in Antarctic Earth Science, Tokyo, Terra Sci. Publ., 67-73.

Shiraishi, K., Ellis, D. J., Hiroi, Y., Fanning, C. M., Motoyoshi, Y. and Nakai, Y., 1994. Cambrian orogenic belt in East Antarctica and Sri Lanka: Implications for Gondwana assembly. J. Geology, 102: 47-65.

Smithson, S. B. and Johnson, R. A., 1989. Crustal structure of the western U. S. based on reflection seismology. In: L. C. Pakiser and W. D. Mooney (Editors), Geophysical Framework of the Continental Unites States. Geol. Soc. Am. Mem., 172: 577-612.

Storey, B. C., 1995. The role of mantle plumes in continental breakup: case histories from Gondwanaland. Nature, 377: 301-308.

Talwani, M., Worzel, J. L. and Landisman, M., 1959. Rapid gravity computations for two-dimensional bodies with application to the Mendicino submarine fracture zone. J. Geophys. Res., 64: 49-59.

Trehu, A. M. and Wheeler, W. H., 1987. Possible evidence for subducted sediments beneath central California. Geology, 15: 254-258.

Tsuboi, S., 1995. POSEIDON. IRIS Newsletter, Arlington, Vol. XIV, 1: 8-9.

Visser, J. and Paulssen, H., 1993. The crustal structure from teleseismic *P*-wave coda-II. Application to data of the NARS array in western Eupore and comparison with deep seismic sounding data. Geophys. J. Int., 112: 26-38.

Wahr, J. M., 1981. Body tides on an elliptical, rotating, elastic and oceanless earth. Geophys. J. R. Astron. Soc., 64: 677-703.

Warner, M., 1990. Basalts, water, or shear zones in the lower continental crust ? In: J. H. Leven, D. M. Finlayson, C. Wright, J. C. Dooley and B. L. N. Kennett (Editors), Seismic Probing of Continents and their Margins. Tectonophysics, 173: 163-174.

Wielandt, E. and Streckeisen, G., 1982. The leaf-spring seismometer, design and performance. Bull. Seismol. Soc. Am., 72: 2349-2367.

Yanai, K. and Kakinuma, S., 1971. Measurement of gravity along the traverse route Syowa-South Pole. In: M. Murayama (Editors), Report of the Japanese Traverse Syowa-South Pole. National Science Museum, Tokyo, 131-150.

Yoshida, M. and Yoshimura, A., 1972. Gravimetric survey in the Mizuho Plateau-West Enderby Land area, East Antarctica, 1969-1971. JARE Data Rep., 17 (Glaciology 1): 168-203.

Zandt, G. and Ammon, C. J., 1995. Continental crust composition constrained by measurements of crustal Poisson's ratio. Nature, 374: 152-154.

Figure Captions

Fig. 1. Geological setting in Eastern Queen Maud Land and Western Enderby Land, East Antarctica, showing the distribution of four distinct metamorphic complexes (modified after Motoyoshi et al, 1989). Syowa Station (SYO) is situated on the Lützow-Holm Complex (LHC). Metamorphic grade increases progressively along the Prince Olav Coast to the Lützow-Holm Bay region (LHB). Transitional zone between amphibolite facies and granulite facies is defined as a first appearance of orthopyroxene in ordinary basic to intermediate gneisses through various reactions.

Fig. 2. Map showing the studied areas in the Lützow-Holm Bay region (LHB), East Antarctica. The shadowed and meshed areas of its center at SYO indicate the surveyed regions by receiver function inversion divided into four backazimuth groups. The group of backazimuth 50°-100° mainly belongs to the transitional zone between amphibolite facies and granulite facies. The 120°-160° backazimuth group is within the granulite facies zone. The other two groups of backazimuth 210°-250° and 300°-360° mainly cover the Lützow-Holm Bay. The bold dashed line shows the reflection section along the Mizuho route between two seismic shot points (SHOT18, 19) in the refraction experiments in 1981. A circle with radius about 120 km of its center at SYO indicates the scattering area affecting the coda wave generation of local earthquakes corresponding to the maximum lapse time of 70 s.

Fig. 3. Comparison of the observed Q_C (Obs.; open circles) and calculated Q_C (Cal.; solid circles with lines) as a function of lapse time for six frequency bands (1, 2, 4, 8, 16 and 24 Hz) in LHB. Averaged values for the observed Q_C (Avrg.) for each lapse time are linked by broken lines. The calculated ones are based on estimation by a one-dimensional Q_S model.

Fig. 4. One-dimensional Q_S model for the crust and uppermost mantle derived from the observed Q_C at various lapse times for six frequency bands. Thickness and Q_S in a layer are

assumed to be constant on the basis of the velocity discontinuities from the *P*-wave velocity model derived from refraction experiments (Ikami et al., 1984).

Fig. 5 Hypocenters of 80 earthquakes (open circles) used in the receiver function inversion for all the backazimuths. Hypocentral distances are restricted within 70°-90° to produce similar incident angles.

Fig. 6. An example of the weighting-stacked radial receiver function before 5 s and after 30 s of *P*-arrival in the 50°-100° backazimuth (the lowest trace; **stacked RF**) together with 26 original observed receiver functions.

Fig. 7. Histogram of delay time from *P*-arrivals of the strong amplitudes with positive correlation grater than 0.2 by applying to all the observed radial receiver functions. Two main peaks are found around 1 s and 4 s; those are considered to be the *Ps* phases from inner crustal and Moho discontinuities.

Fig. 8. An example of shear velocity models down to 60 km depth by receiver function inversion using different one-dimensional Q_S model of 1, 2 and 4 Hz (solid-bold lines; 1Hz, solid-thin lines; 2Hz, dashed lines; 4Hz) in 50°-100° backazimuth. An initial velocity model by refraction experiments (Ikami et al., 1984) is also presented by the broken line.

Fig. 9a. Shear wave velocity model down to 60 km depth by receiver function inversion in the 50°-100° backazimuth (open circles with solid line). Error bars are +/- 1 standard errors. The initial velocity model is presented by the thin-broken line.

Fig. 9b. Synthetic radial receiver function (broken traces) compared to observed mean (upper solid trace) and +/- 1 standard error bounding (lower two solid traces) of weighting-stacked radial receiver functions up to 30 s from the *P*-arrival in the 50°-100° backazimuths. The number of original observed traces for stacking is shown as the 'No.' value.

Fig. 10a. Shear wave velocity model by receiver function inversion in the 120°-160° backazimuth. Same display scheme as Fig. 8a.

Fig. 10b. Synthetic radial receiver function compared to observed mean and standard error bounding of weighting-stacked receiver functions in the 120°-160° backazimuths. Same display scheme as Fig. 8b.

Fig. 11a. Shear wave velocity model by receiver function inversion in the 210°-250° backazimuth. Same display scheme as Fig. 8a.

Fig. 11b. Synthetic radial receiver function compared to observed mean and standard error bounding of weighting-stacked receiver functions in the 210°-250° backazimuths. Same display scheme as Fig. 8b.

Fig. 12a. Shear wave velocity model by receiver function inversion in the 300°-360° backazimuth. Same display scheme as Fig. 8a.

Fig. 12b. Synthetic radial receiver function compared to observed mean and standard error bounding of weighting-stacked receiver functions in the 300°-360° backazimuths. Same display scheme as Fig. 8b.

Fig. 13. A reflected record section of SHOT 19 with the band-pass filter of 8-15 Hz after normal-moveout correction. There are clear phases of large amplitudes in a range of 8-16 s of two-way travel time. The shadowed area shows the reflective zones corresponding to the lower crust (after Ito and Kanao, 1995).

Fig. 14. Schematic illustration of the crustal structure along the Mizuho routes (after Ito and Kanao, 1995). The depths of representative reflected layers (dashed lines in the lower figure)

are superposed in the *P*-wave velocity model by the refraction experiments along the Mizuho routes (Ikami et al., 1984). Numerals in layers indicate *P*-wave velocities in km/s. Surface elevation, free-air and Bouguer gravity anomalies along the routes are after Shimizu et al. (1972), Yoshida and Yoshimura (1972), Abe (1975) and Kamiyama et al. (1994).

Fig. 15a. Shear velocity model by receiver function inversion in the 50°-100° backazimuth (solid line) and the velocity laminated model for forward estimation to produce the synthetic receiver functions (dashed line). Laminated layers are assumed in the lower crustal depth with 1.0 km thickness.

Fig. 15b. Synthetic radial receiver function computed from the final model of the inversion (upper broken trace), synthetic one computed from the model of velocity laminated layers (lower broken trace) compared to +/- 1 standard error bounding (two solid traces) of weighting-stacked receiver functions in the 50°-100° backazimuths.

Fig. 16. Map of Prince Olav and Soya Coasts, showing the boundary between the two Complexes of Rayner and Lūtzow-Holm, their metamorphic facies and the location of metastable kyanite, Sp.75020609, isograds, and the thermal axis. S, Syowa Station; M, Molodezhnaya Station (after Hiroi et al., 1991).

Fig. 17. Schematic NE-SW cross-section illustrating an interpretation of the relationships between the Napier Complex, the Rayner Complex and LHC in western Enderby Land and Eastern Queen Maud Land. Late Proterozoic structures are interpreted to have caused initial uplift and exhumation of the Napier Complex; Cambrian and perhaps more recent faultings are believed to have resulted in sufficient thickening to cause later exposure through erosion (after Harley and Hensen, 1990).

Fig. 18. Shear wave velocity models by receiver function inversion in the two continental backazimuth groups of 50°-100° and 120°-160° (Vs; bold broken lines), average velocity

model for shields and platforms (**Vs_Shields**; solid squares with lines) compared to averaged laboratory measured velocities in metamorphic rocks (after Cristensen and Mooney, 1995). Rock abbreviations are as follows. GGN; Granite Gneiss, BGN; Biotite (Tonalite) Gneiss, AMP; Amphibolite, FGR; Felsic Granulite, PGR; Paragranulite, AGR; Anorthositic Granulite, MGR; Mafic Granulite, GGR; Mafic Garnet Granulite, ECL; Mafic Eclogite.

Fig. 19. Splitting parameters versus backazimuth for Moho *Ps* phases (open circles; after Kanao et al., 1996) and *SKS* phases (solid circles; after Kubo et al., 1995). The fastest directions (upper figure) are averaged over N133°E (Moho *Ps*) and in N49°E (*SKS*), and the arrival time difference between fast and slow polarized waves (lower figure) is averaged over 0.5 s (Moho *Ps*) and in 0.7 s (*SKS*), respectively.

Table 1. List of teleseismic earthquakes used in the receiver function inversion for all the backazimuths (**Inc. angle**; incident angle, **stack_wt.**; weight for stacking of observed receiver functions). The total number of traces is 80. Mb denotes the earthquake magnitude determined by USGS.

Table 2. List of model parameters in the receiver function inversion. The initial velocity model, constraints of upper- and lower-limit of the inversion, ratio of *P*- to *S*- wave velocities (V_P/V_S) and the attenuation factor for *P*- and *S*- waves (Q_P, Q_S) are presented in 32 layers.

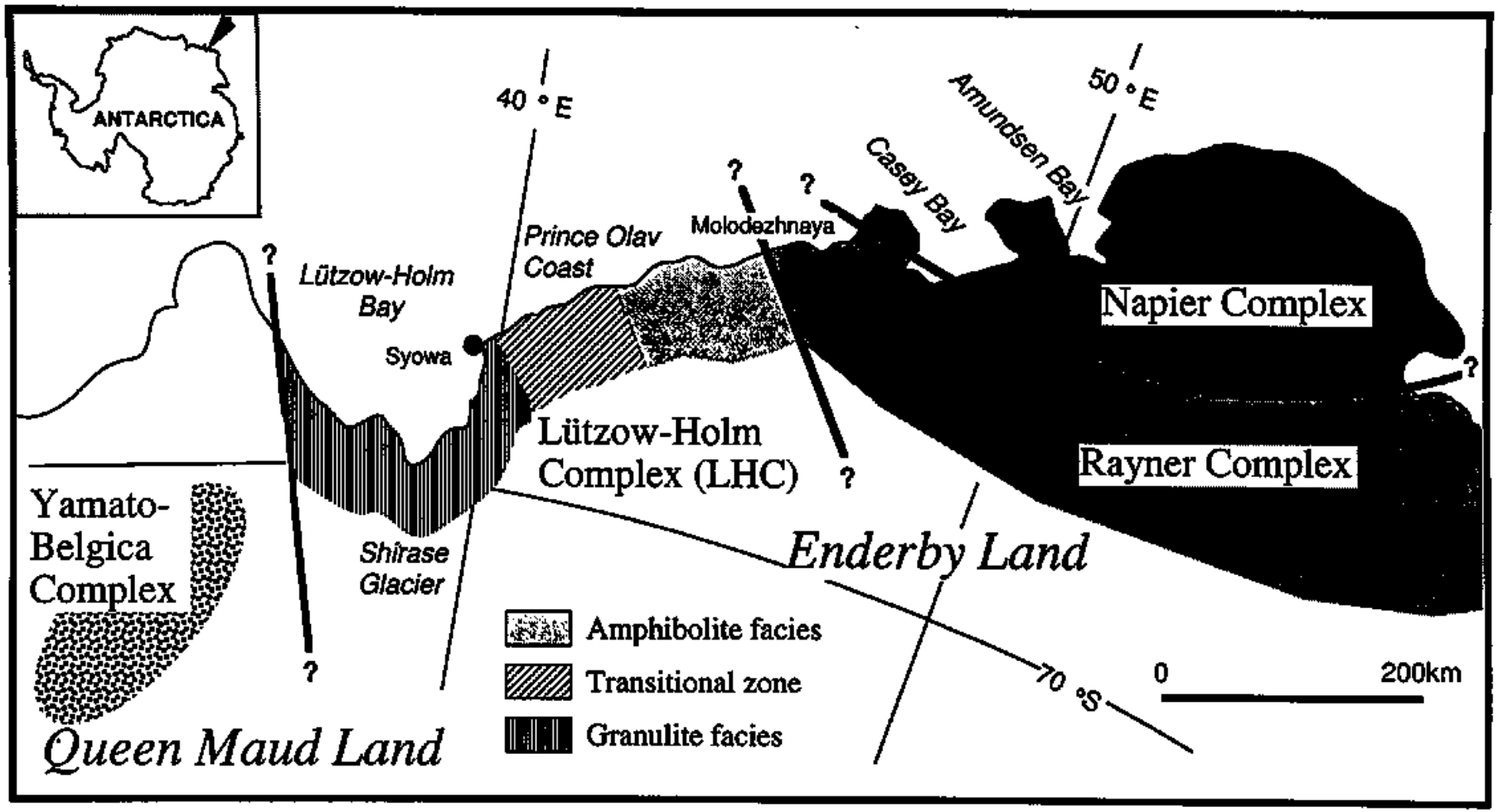
ANTARCTICA
40 °E
50 °E
Amundsen Bay
Casey Bay
Molodezhnaya
Prince Olav Coast
Lützow-Holm Bay
Syowa
Napier Complex
Rayner Complex
Lützow-Holm Complex (LHC)
Enderby Land
Yamato-Belgica Complex
Shirase Glacier
Queen Maud Land
Amphibolite facies
Transitional zone
Granulite facies
70 °S
0
200km

M. Kanao Fig. 1.

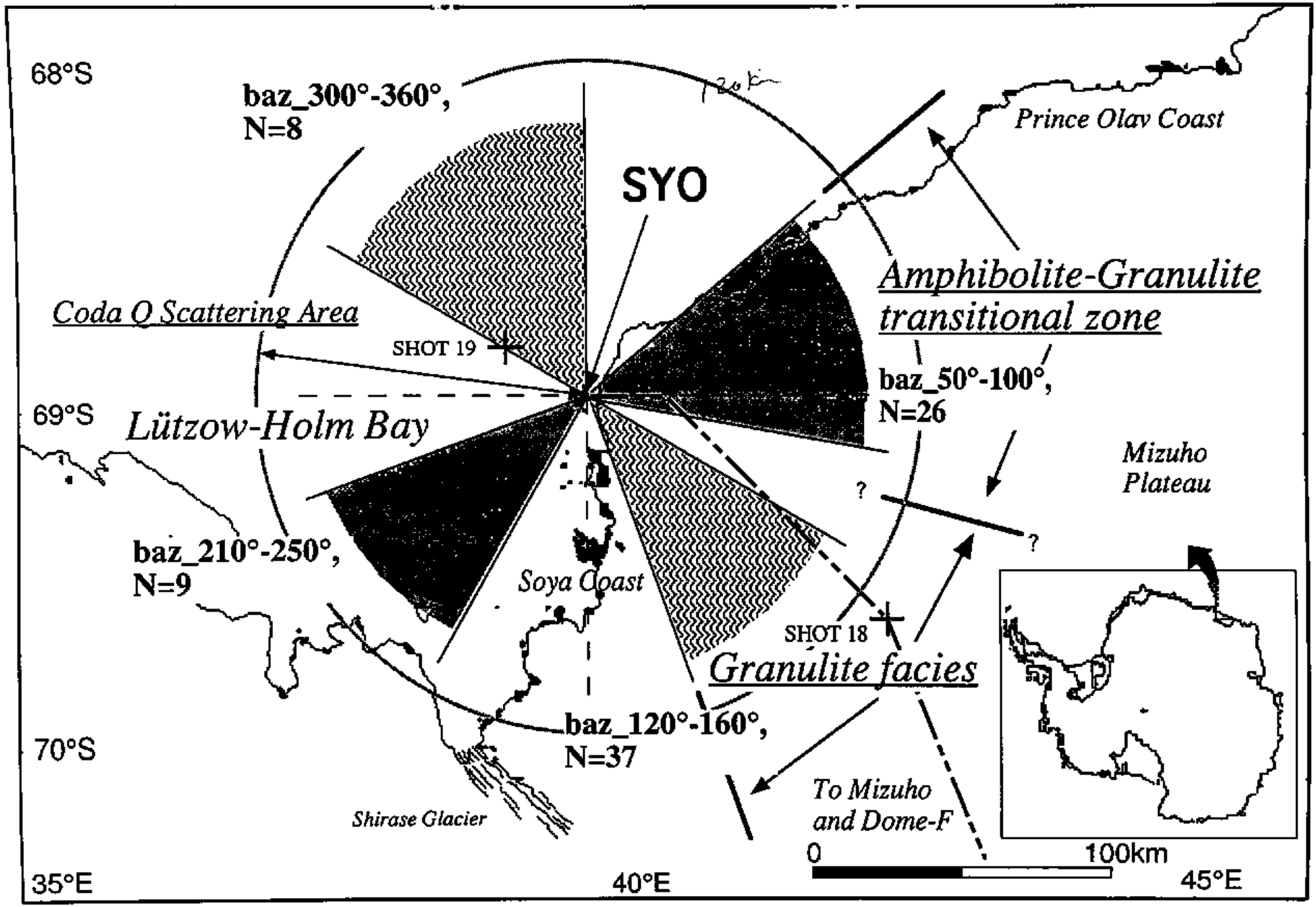
68°S
baz_300°-360°,
N=8
SYO
Prince Olav Coast
Amphibolite-Granulite
transitional zone
Coda Q Scattering Area
SHOT 19
baz_50°-100°,
N=26
69°S
Lützow-Holm Bay
Mizuho
Plateau
?
?
baz_210°-250°,
N=9
Soya Coast
SHOT 18
Granulite facies
baz_120°-160°,
N=37
70°S
To Mizuho
and Dome-F
Shirase Glacier
0
100km
35°E
40°E
45°E

M. Kanao ***Fig. 2.***

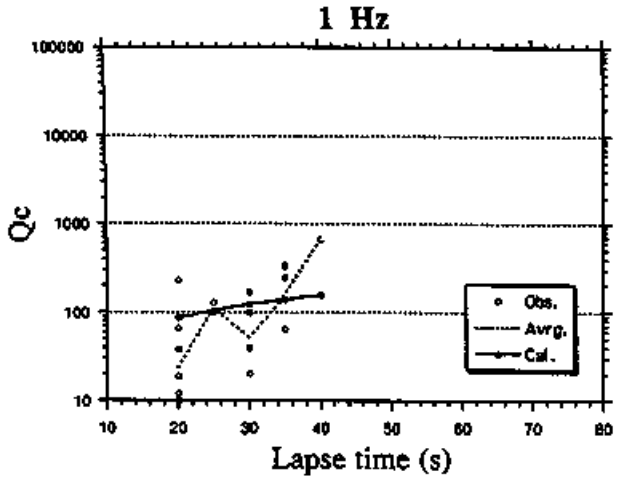
1 Hz
Qc
Lapse time (s)
Obs.
Avrg.
Cal.

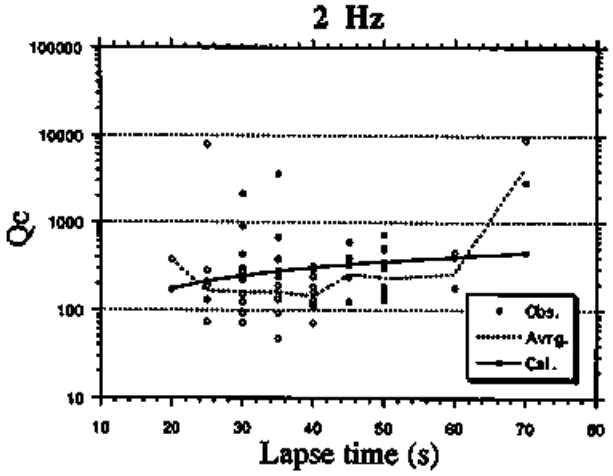
2 Hz
Qc
Lapse time (s)
Obs.
Avrg.
Cal.

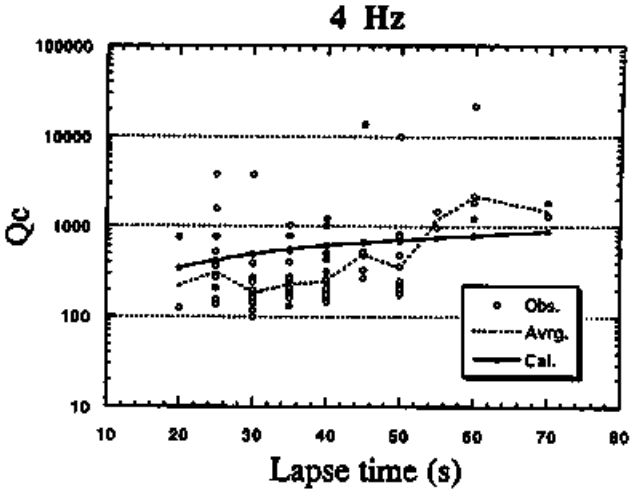
4 Hz
Qc
Lapse time (s)
Obs.
Avrg.
Cal.

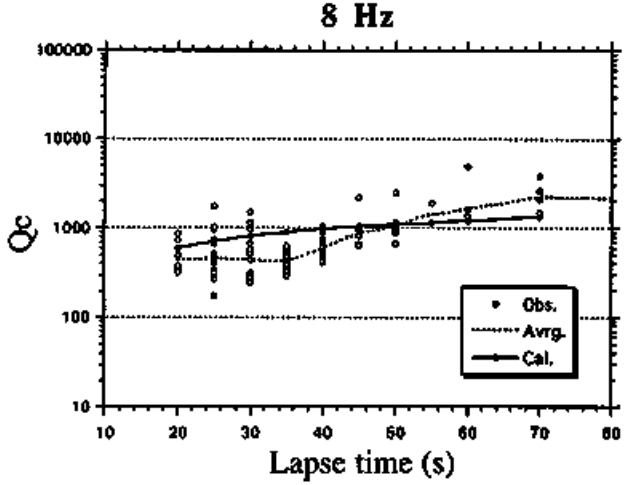
8 Hz
Qc
Lapse time (s)
Obs.
Avrg.
Cal.

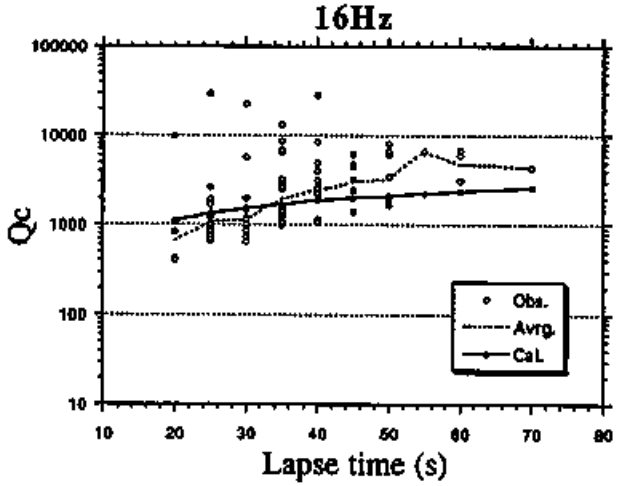
16Hz
Qc
Lapse time (s)
Obs.
Avrg.
Cal.

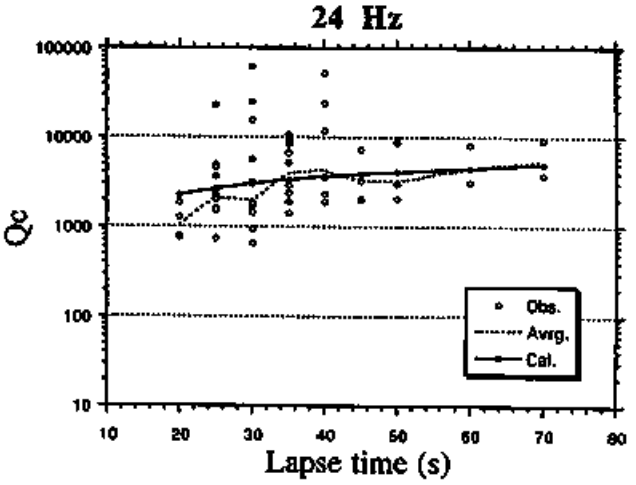
24 Hz
Qc
Lapse time (s)
Obs.
Avrg.
Cal.

M. Kanao Fig. 3.

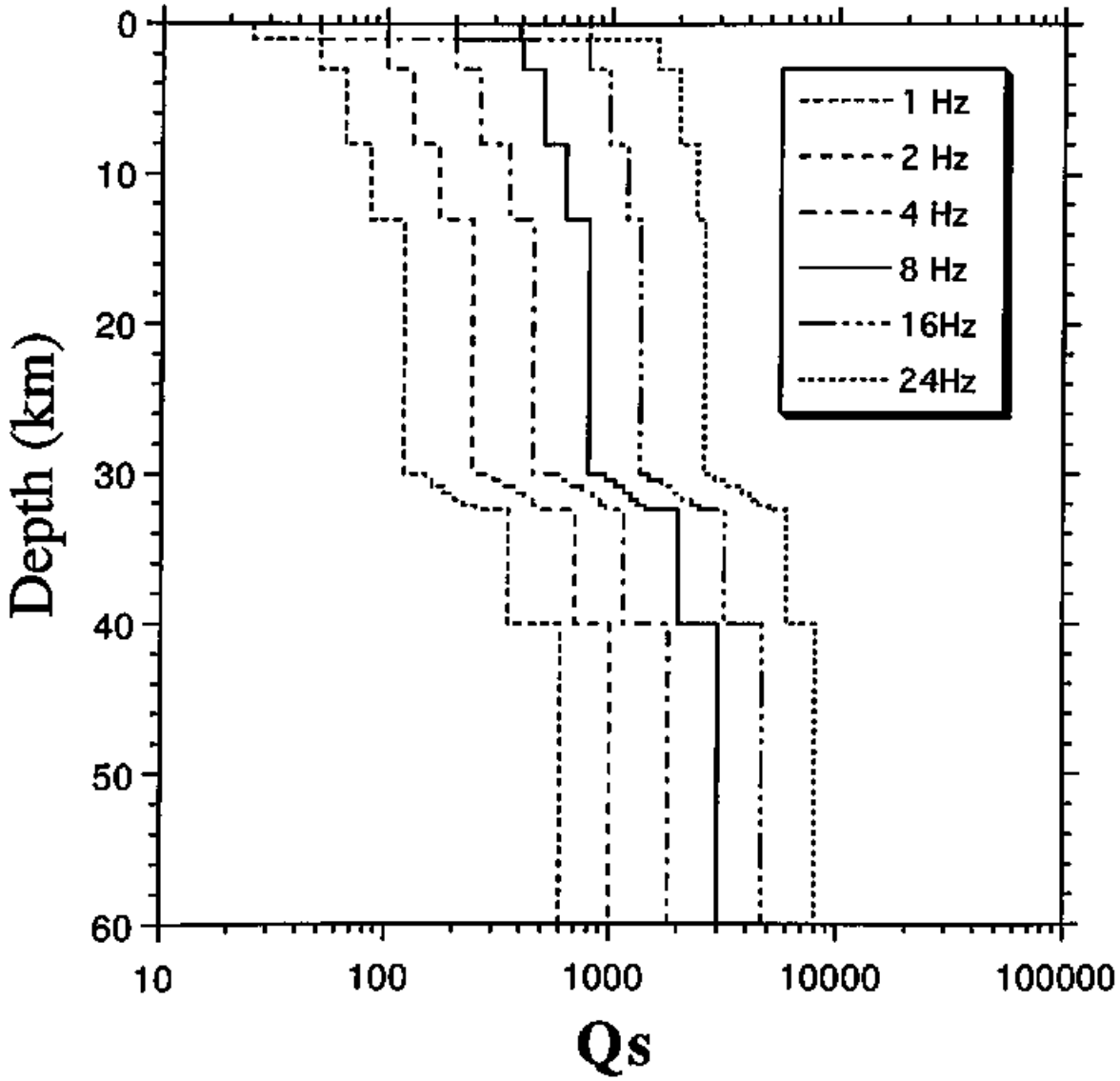
0
10
20
30
40
50
60
Depth (km)
10
100
1000
10000
100000
Qs
1 Hz
2 Hz
4 Hz
8 Hz
16Hz
24Hz

M. Kanao Fig. 4.

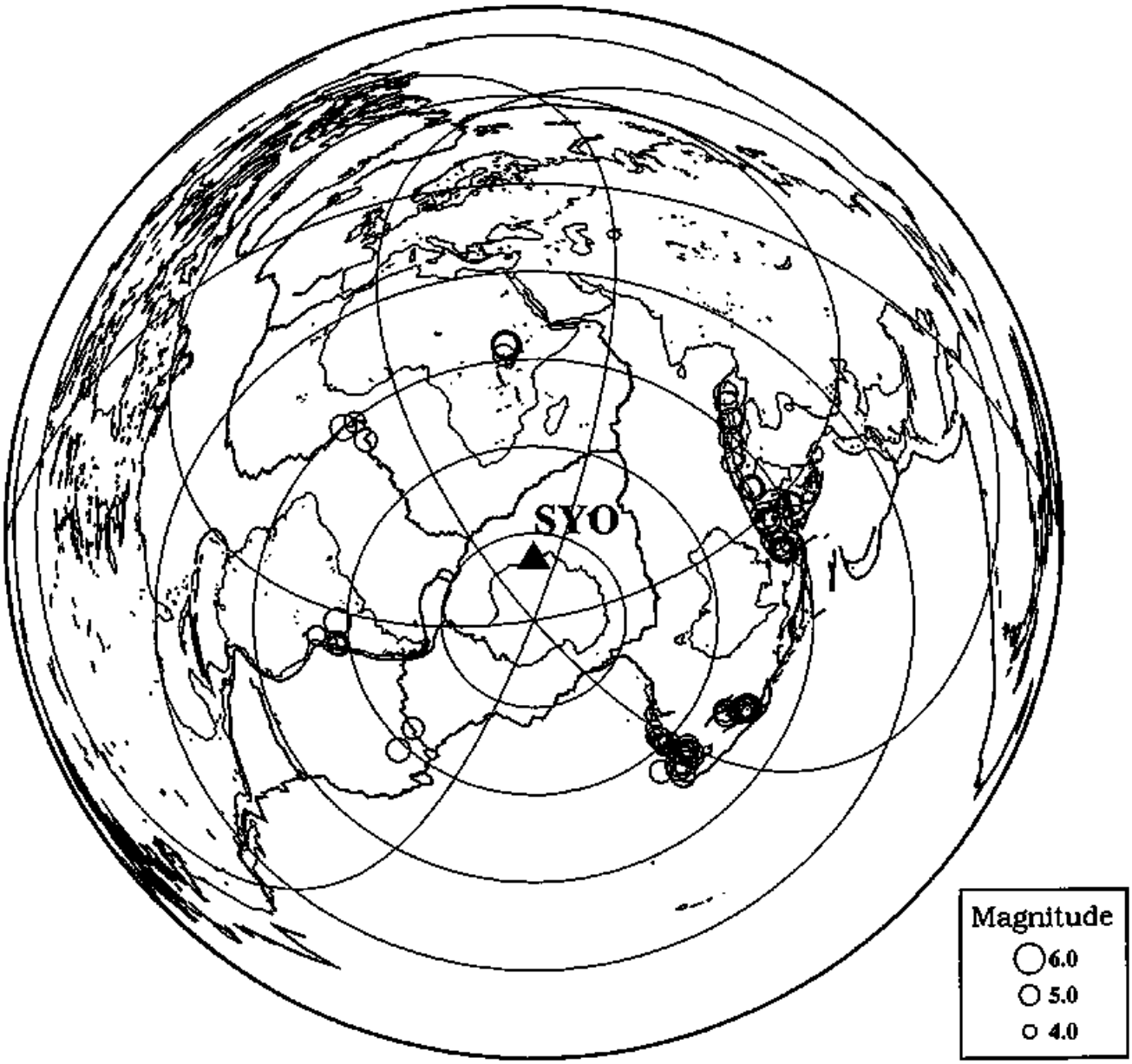

M. Kanao Fig. 5.

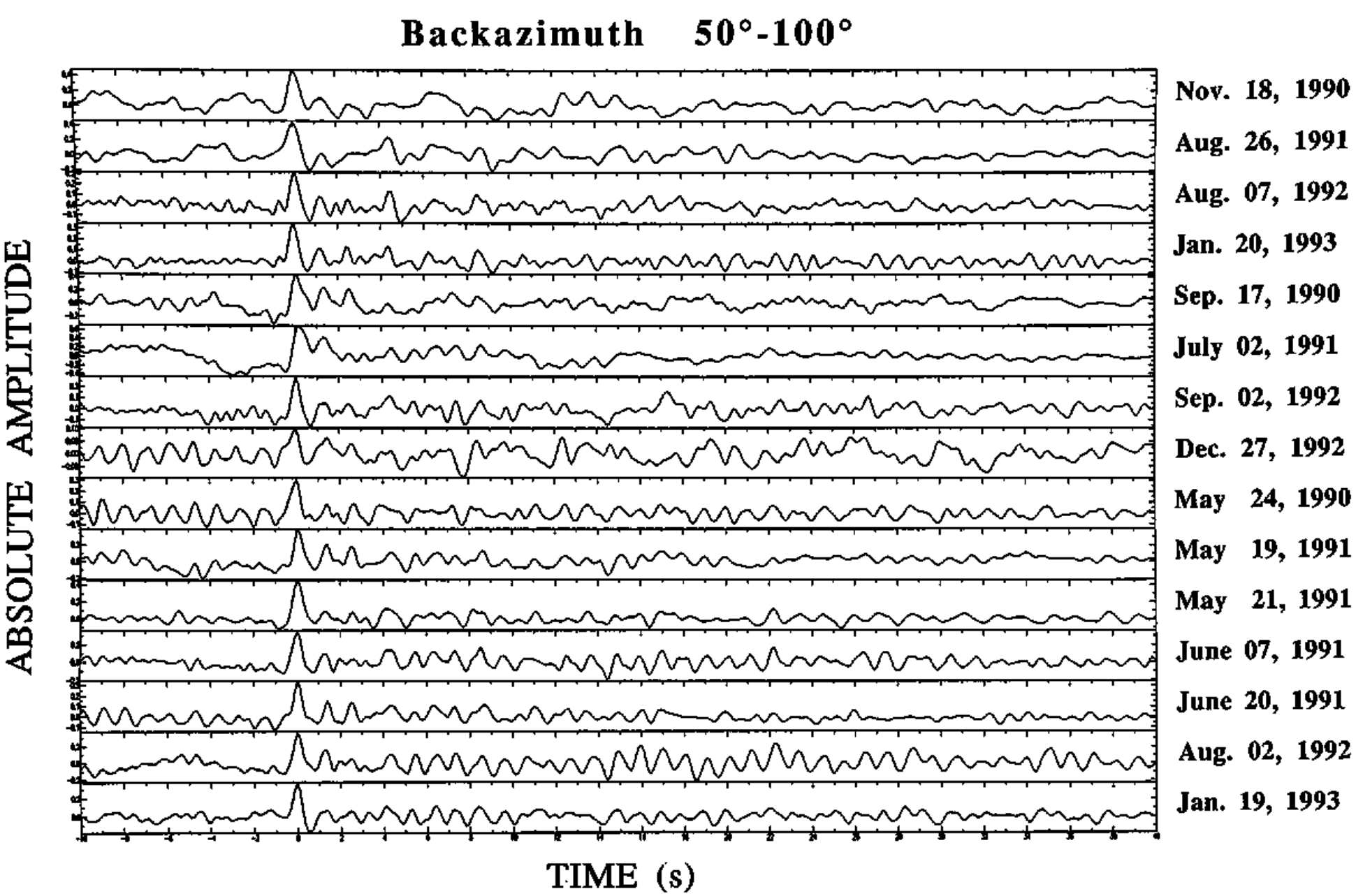
Backazimuth 50°-100°
ABSOLUTE AMPLITUDE
Nov. 18, 1990
Aug. 26, 1991
Aug. 07, 1992
Jan. 20, 1993
Sep. 17, 1990
July 02, 1991
Sep. 02, 1992
Dec. 27, 1992
May 24, 1990
May 19, 1991
May 21, 1991
June 07, 1991
June 20, 1991
Aug. 02, 1992
Jan. 19, 1993
TIME (s)

M. Kanao Fig. 6.

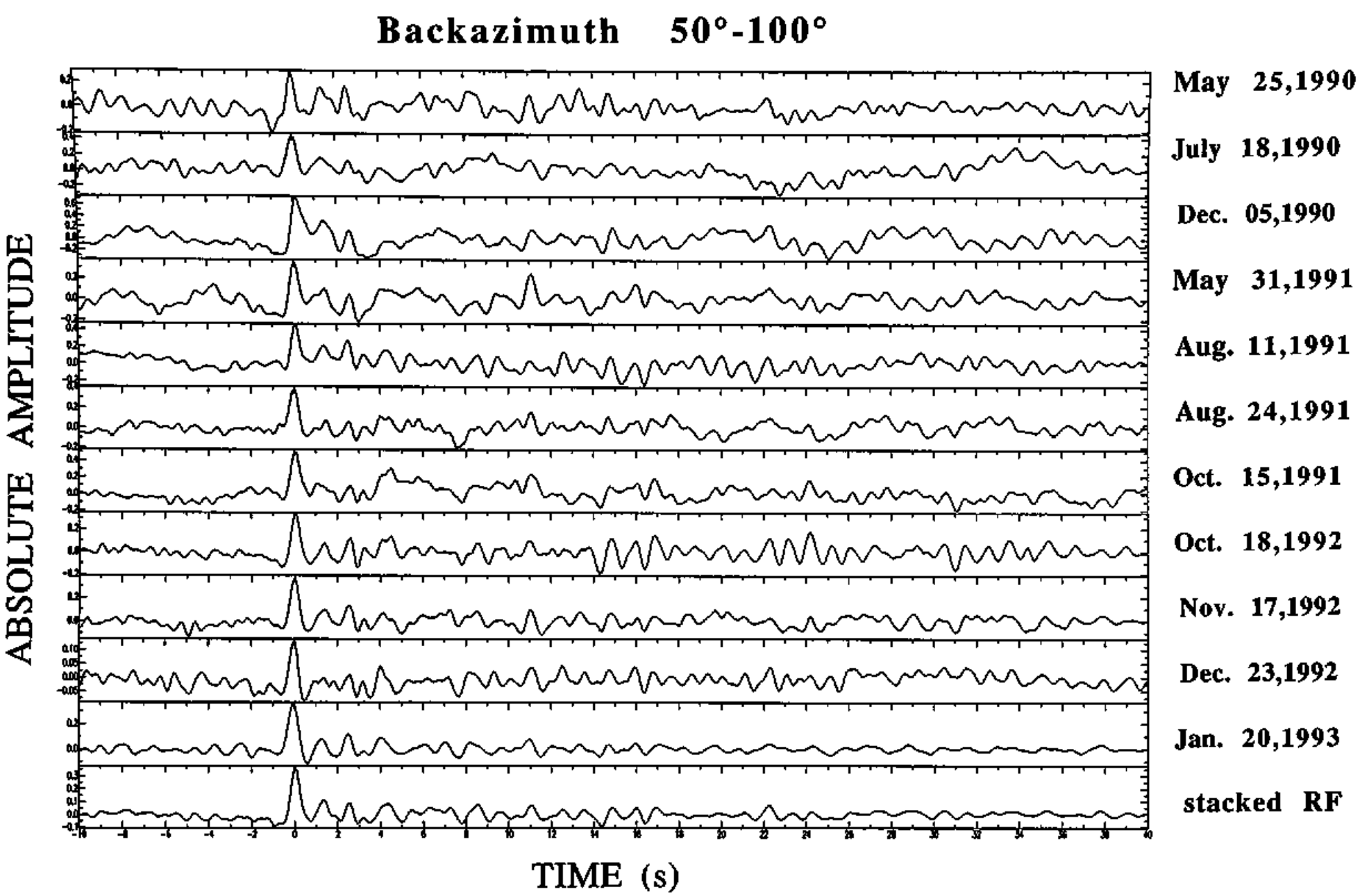

M. Kanao ***Fig. 6. (continued)***

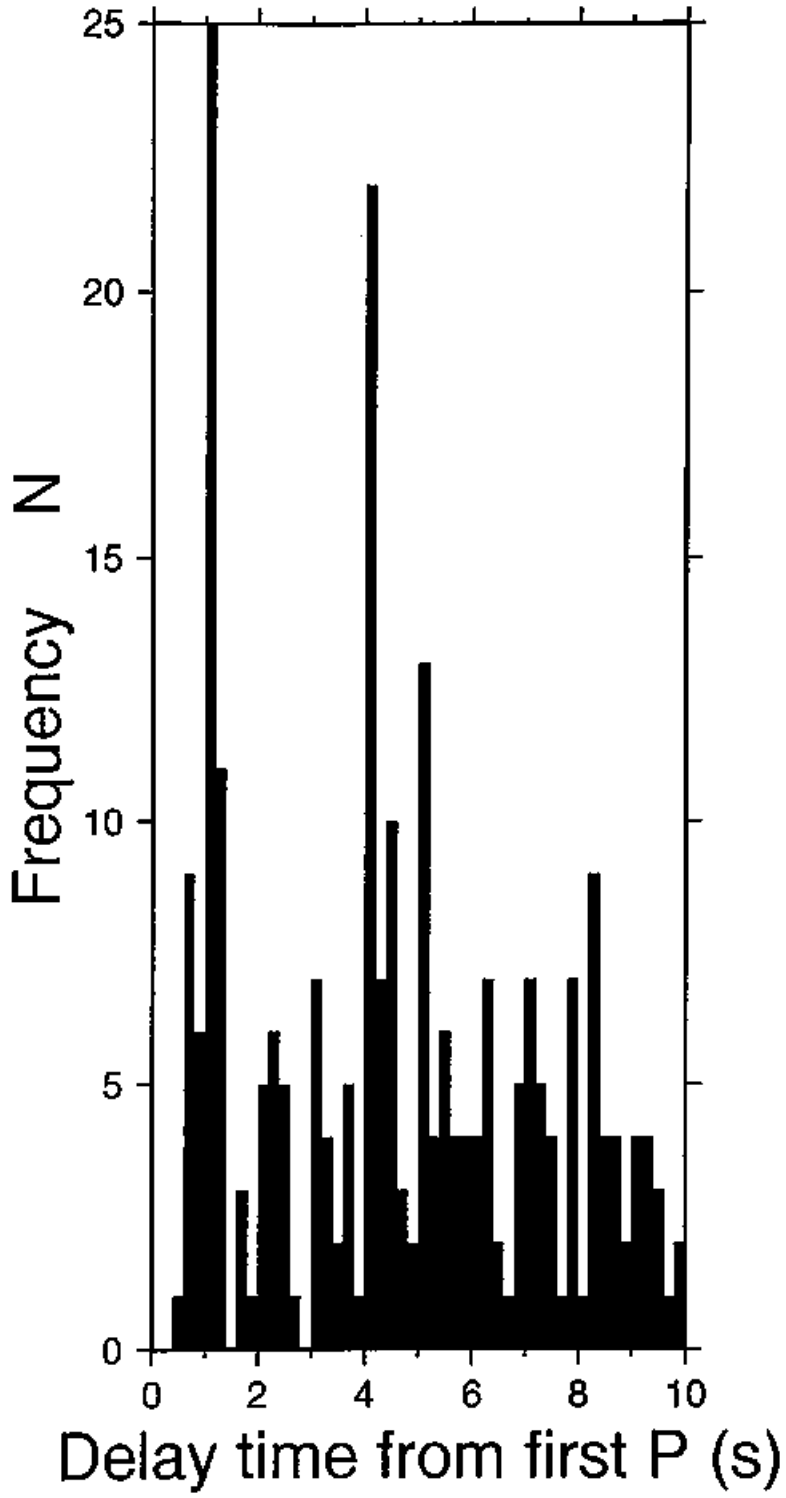

M. Kanao Fig. 7.

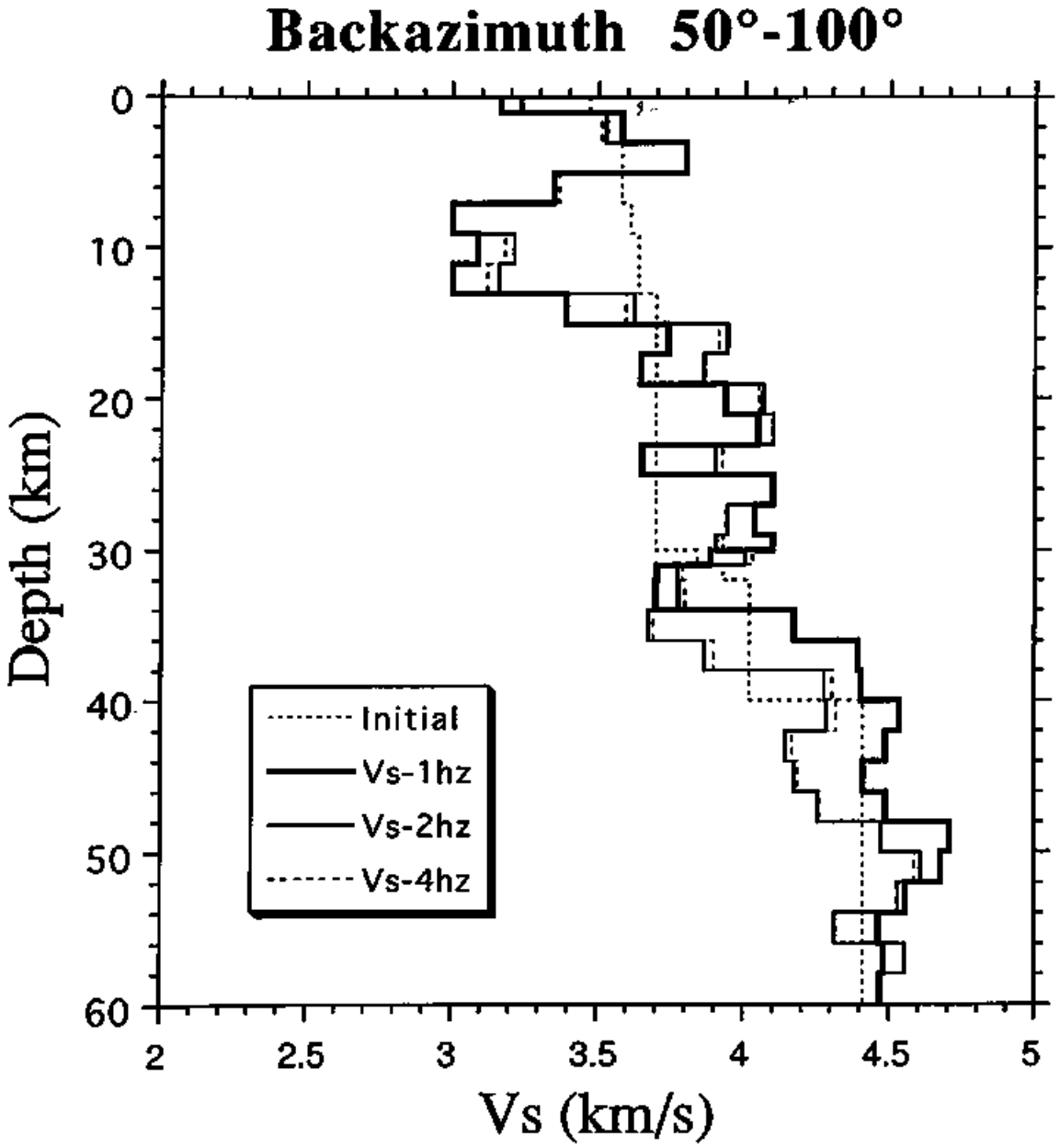
Backazimuth 50°-100°
Depth (km)
0
10
20
30
40
50
60
2
2.5
3
3.5
4
4.5
5
Vs (km/s)
Initial
Vs-1hz
Vs-2hz
Vs-4hz

M. Kanao Fig. 8.

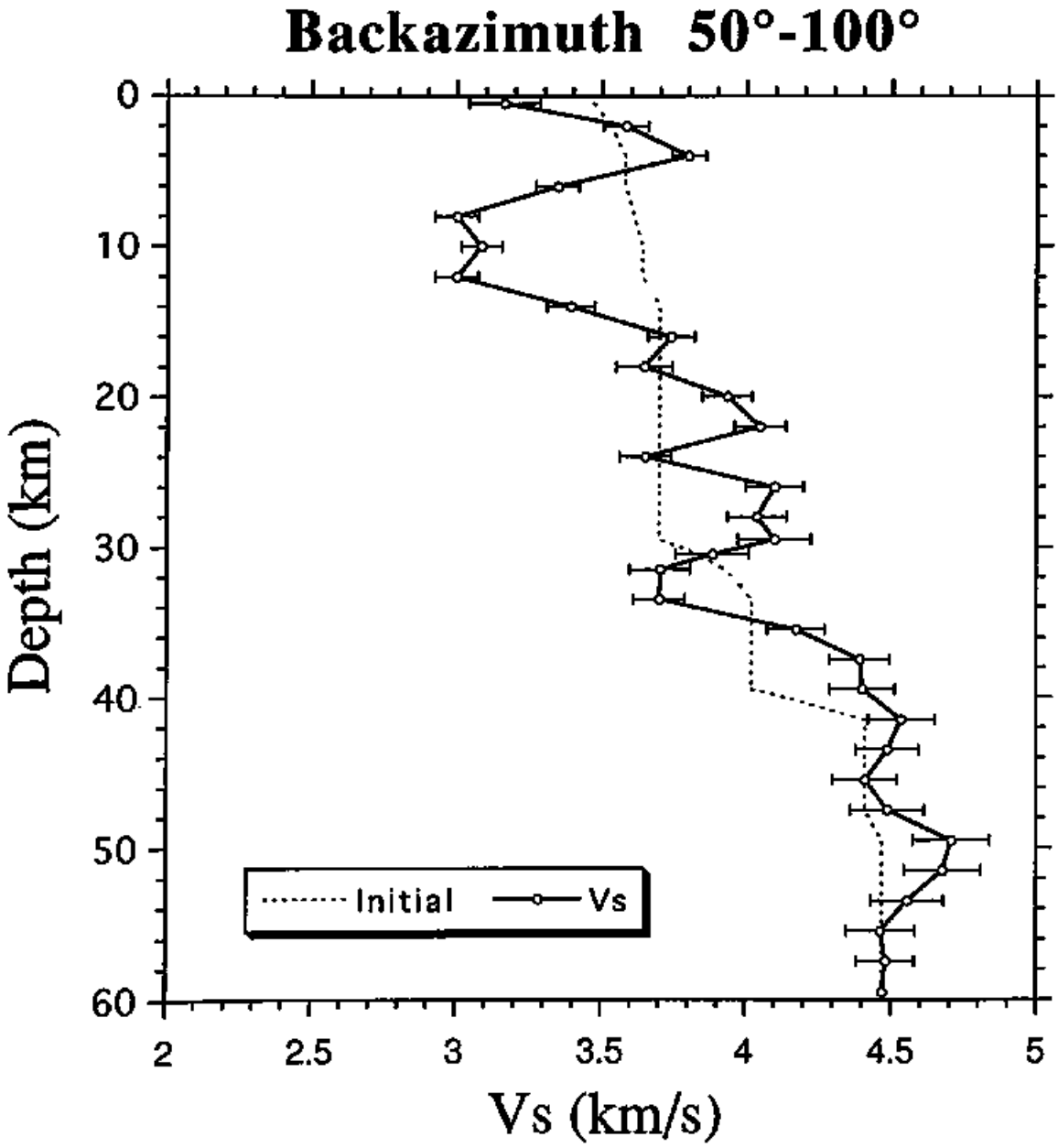

M. Kanao Fig. 9a.

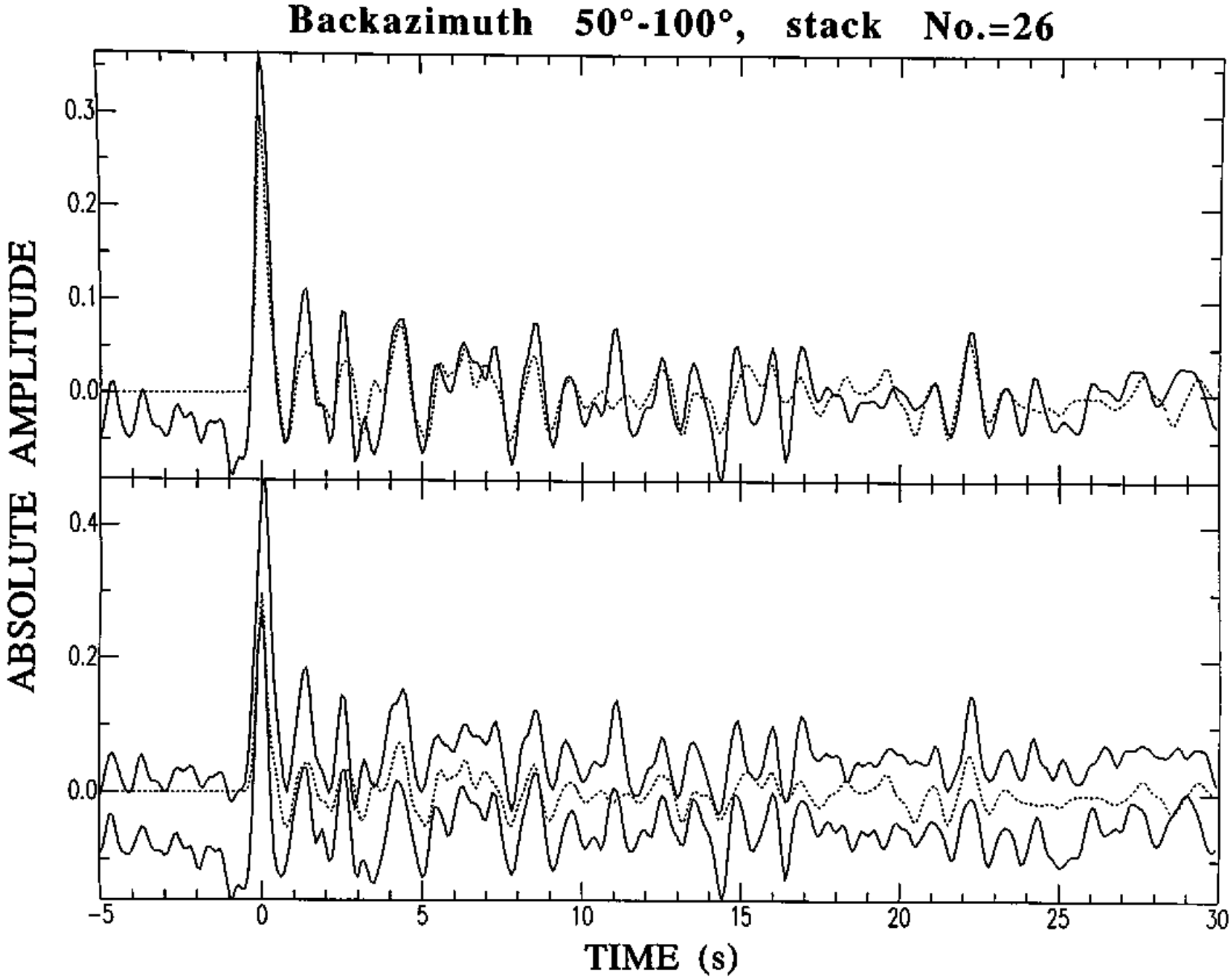

M. Kanao *Fig. 9b.*

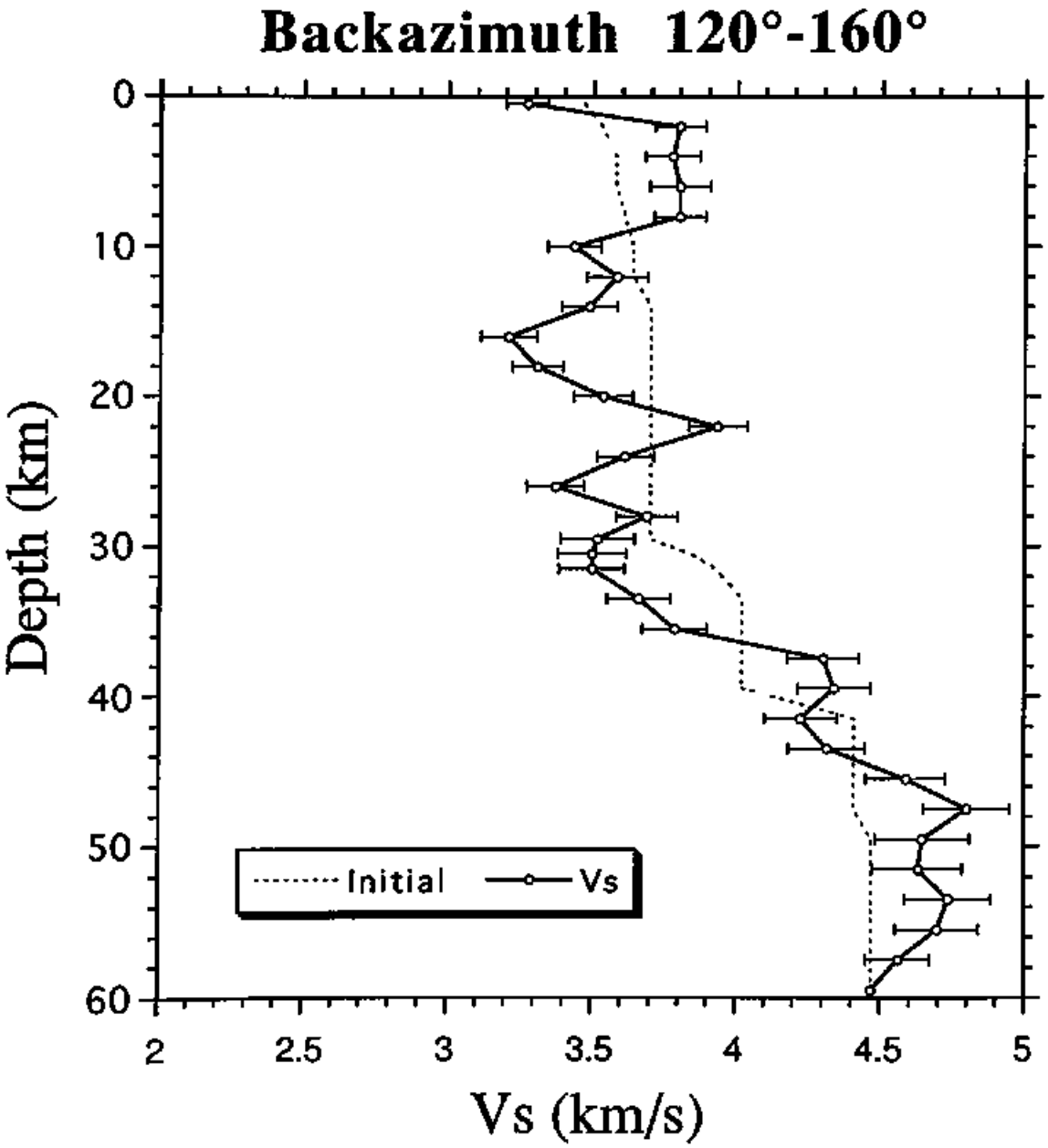

M. Kanao Fig. 10a.

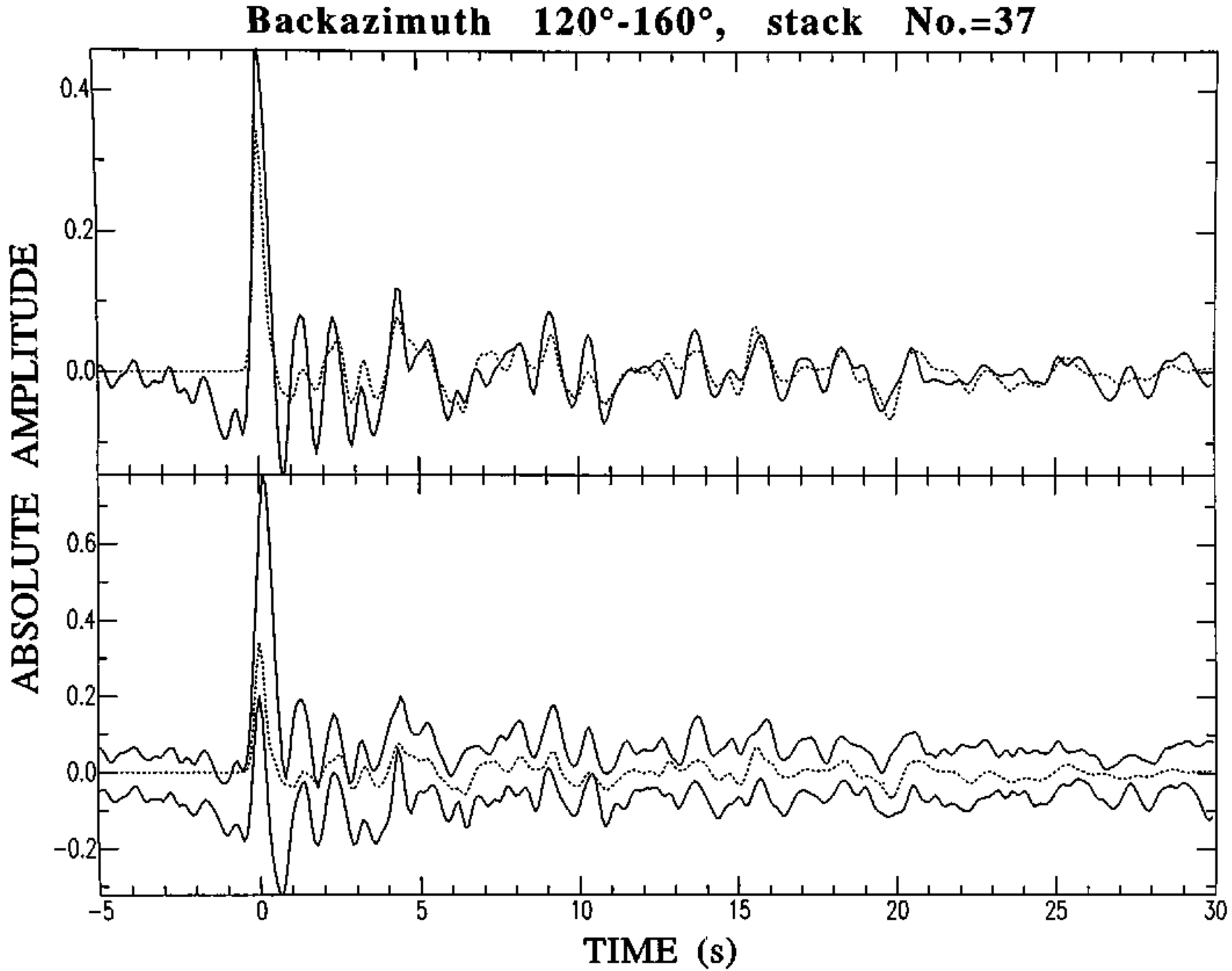
Backazimuth 120°-160°, stack No.=37
ABSOLUTE AMPLITUDE
0.4
0.2
0.0
0.6
0.4
0.2
0.0
-0.2
-5
0
5
10
15
20
25
30
TIME (s)

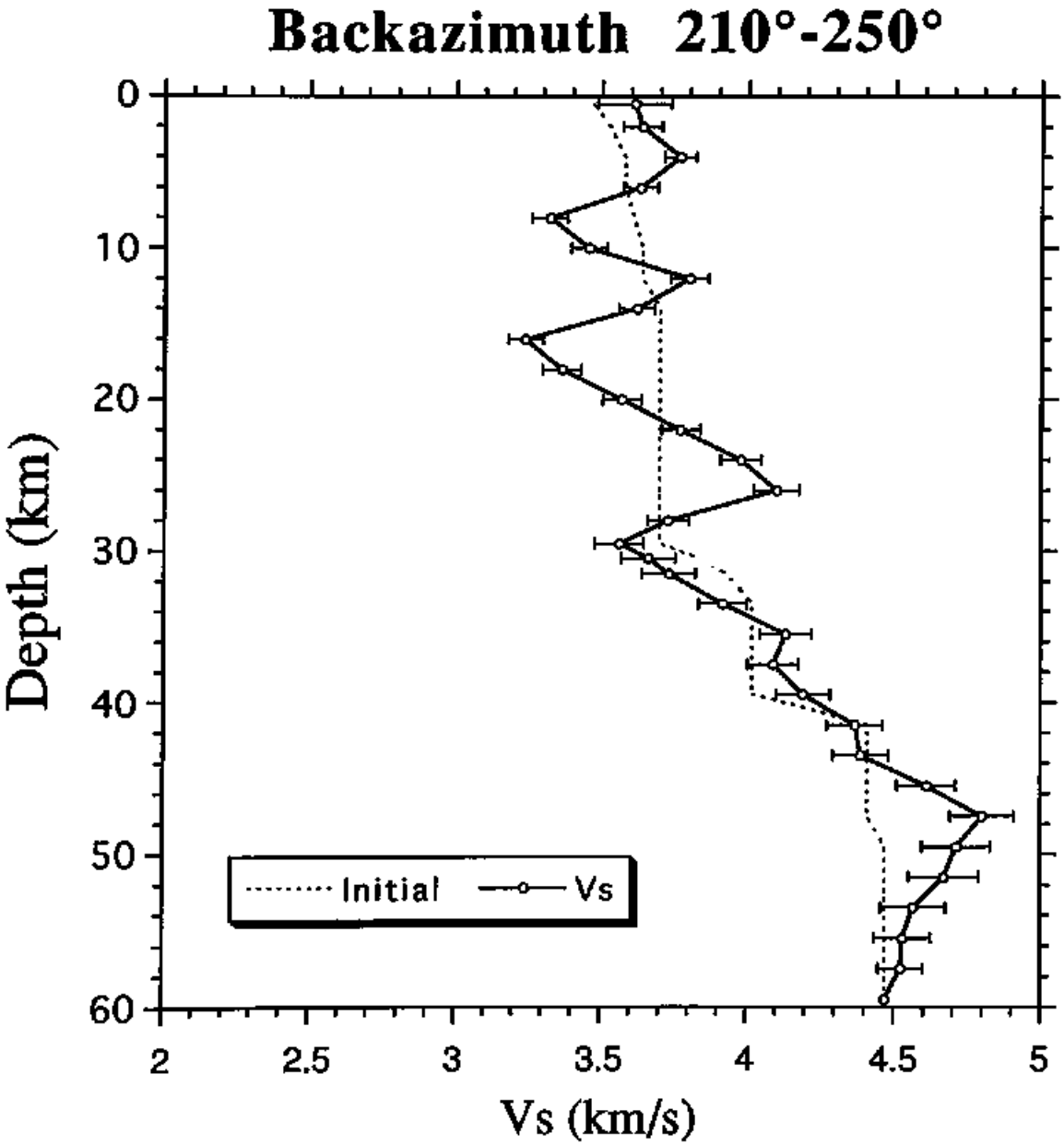

M. Kanao Fig. 11a.

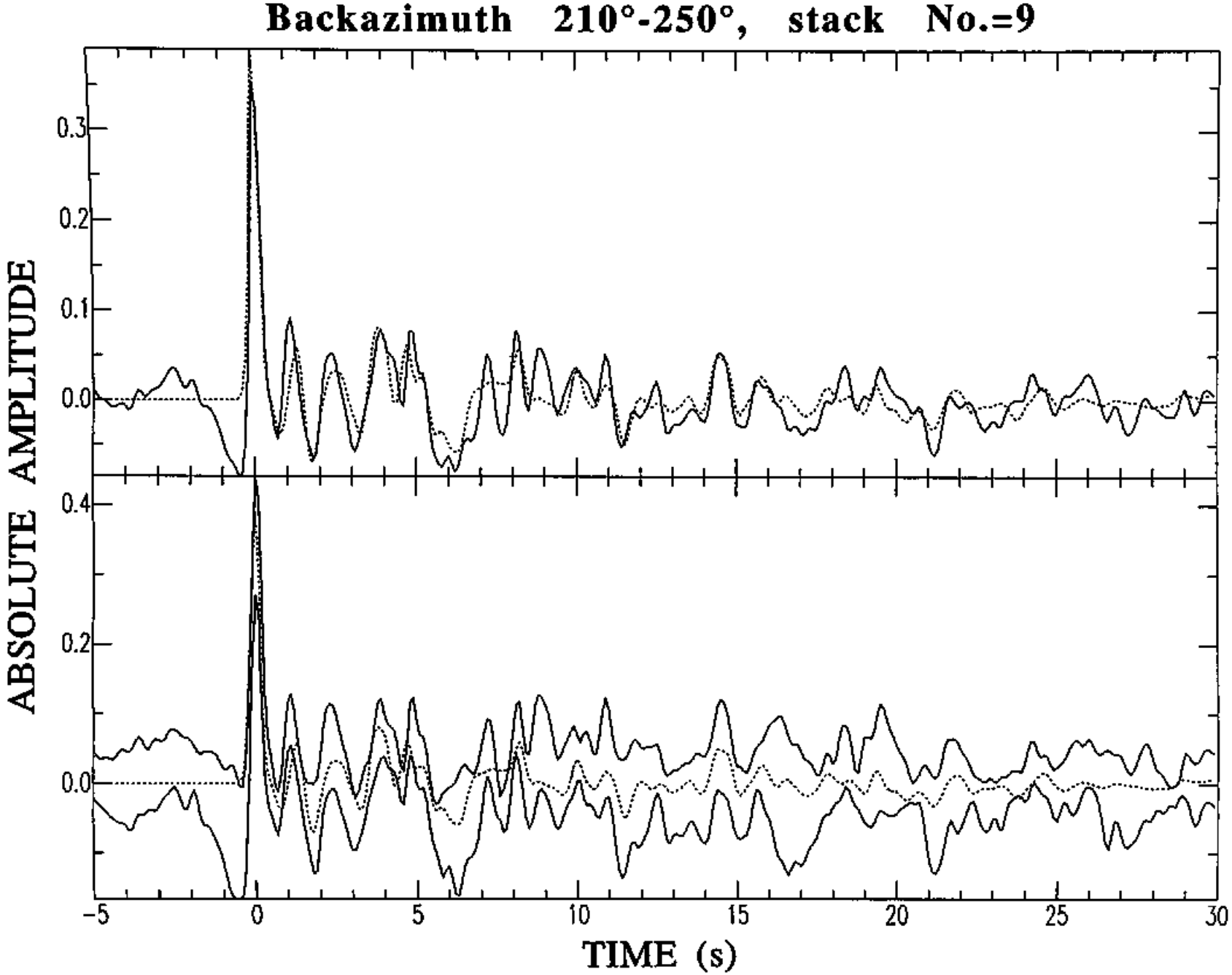
Backazimuth 210°-250°, stack No.=9
ABSOLUTE AMPLITUDE
0.3
0.2
0.1
0.0
0.4
0.2
0.0
-5
0
5
10
15
20
25
30
TIME (s)

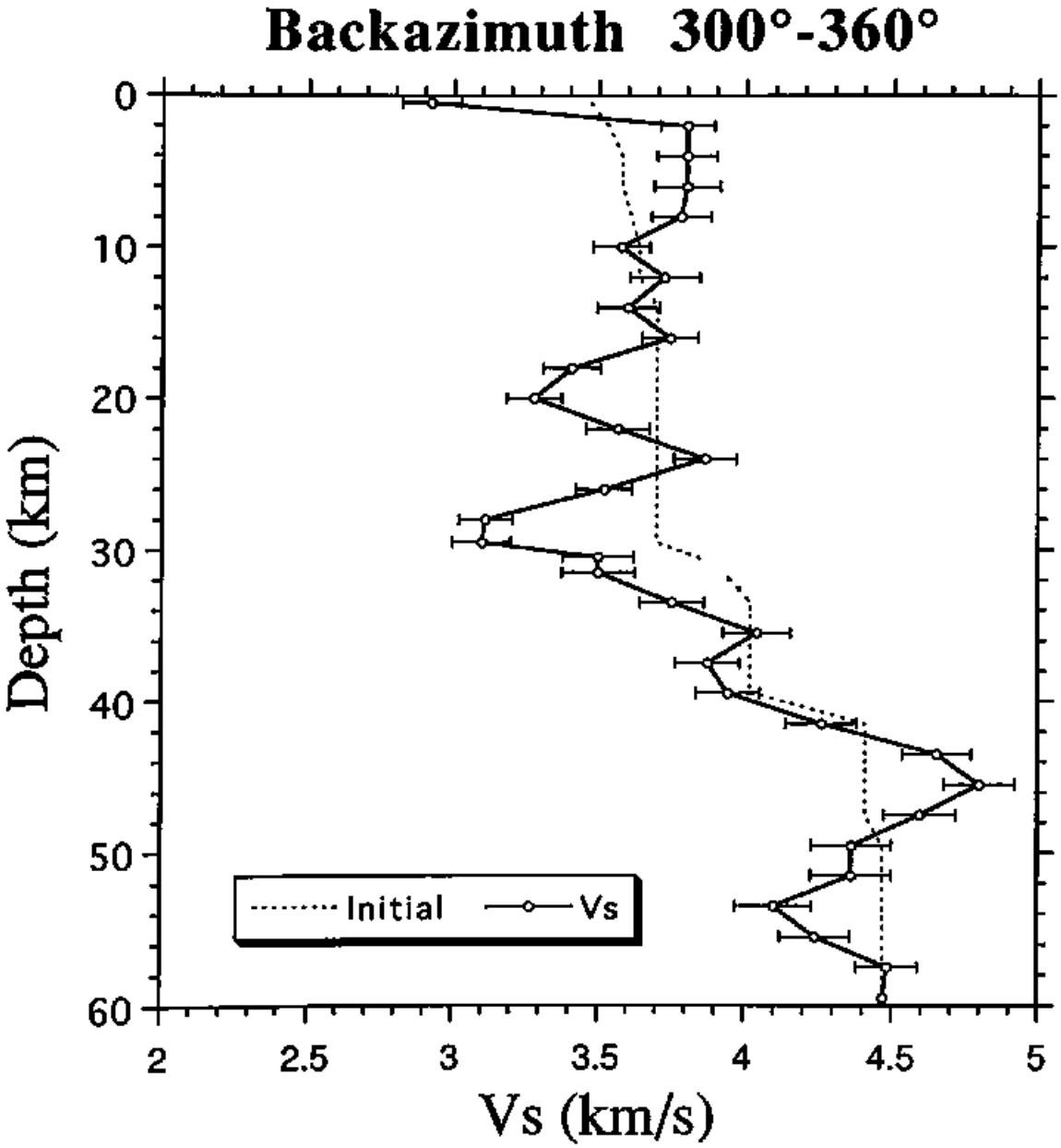

M. Kanao Fig. 12a.

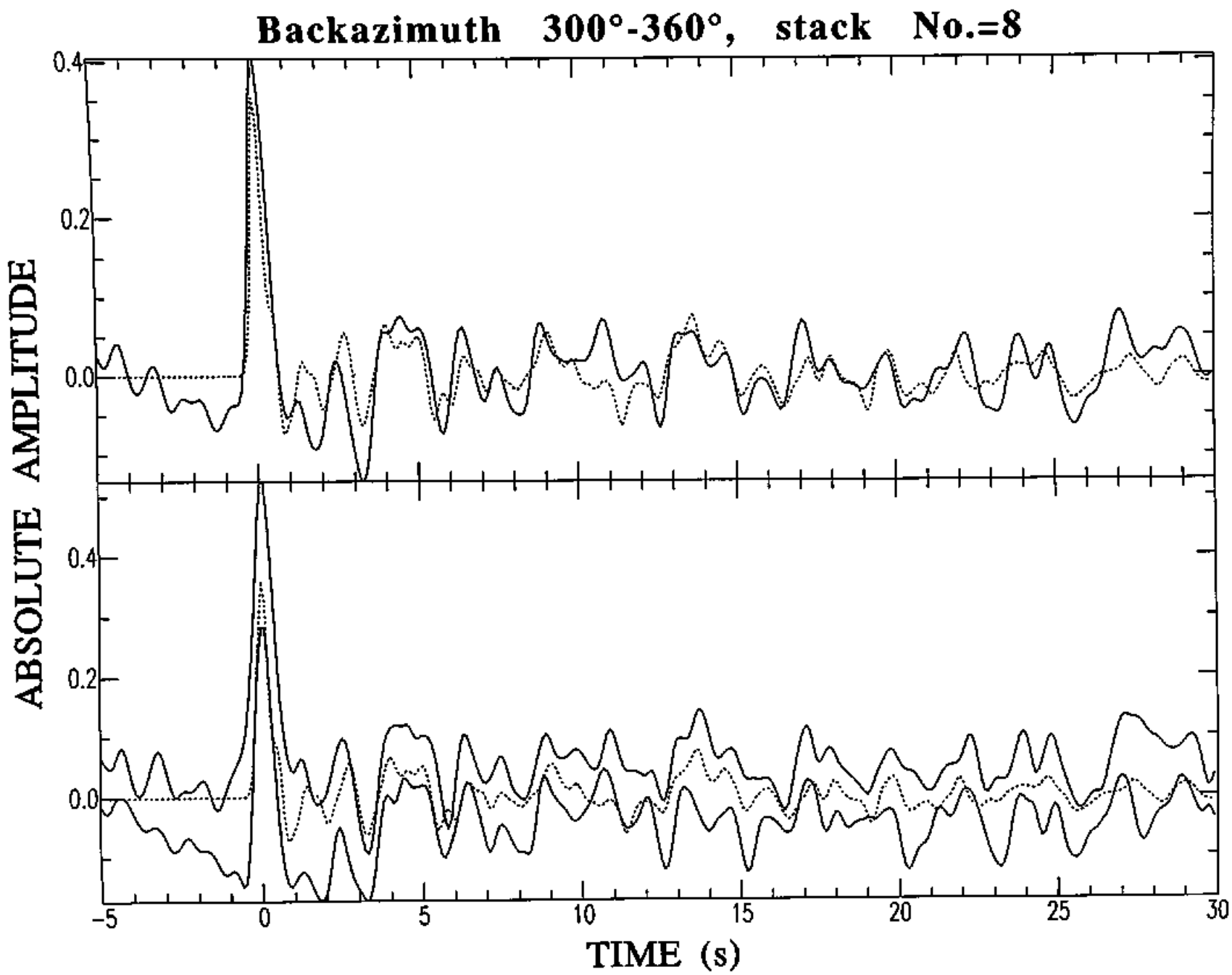
Backazimuth 300°-360°, stack No.=8
ABSOLUTE AMPLITUDE
0.4
0.2
0.0
0.4
0.2
0.0
-5
0
5
10
15
20
25
30
TIME (s)

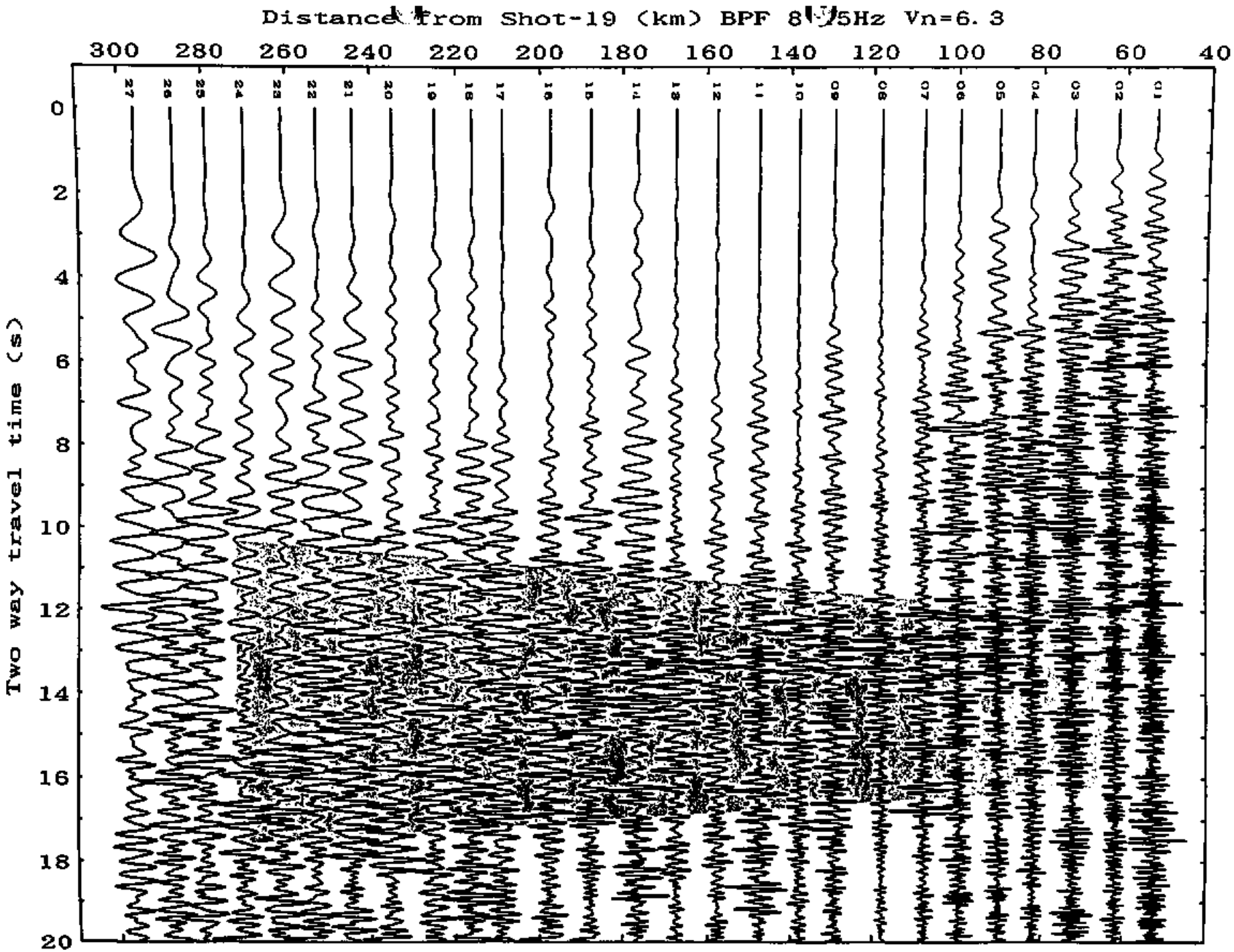

M. Kanao Fig. 13.

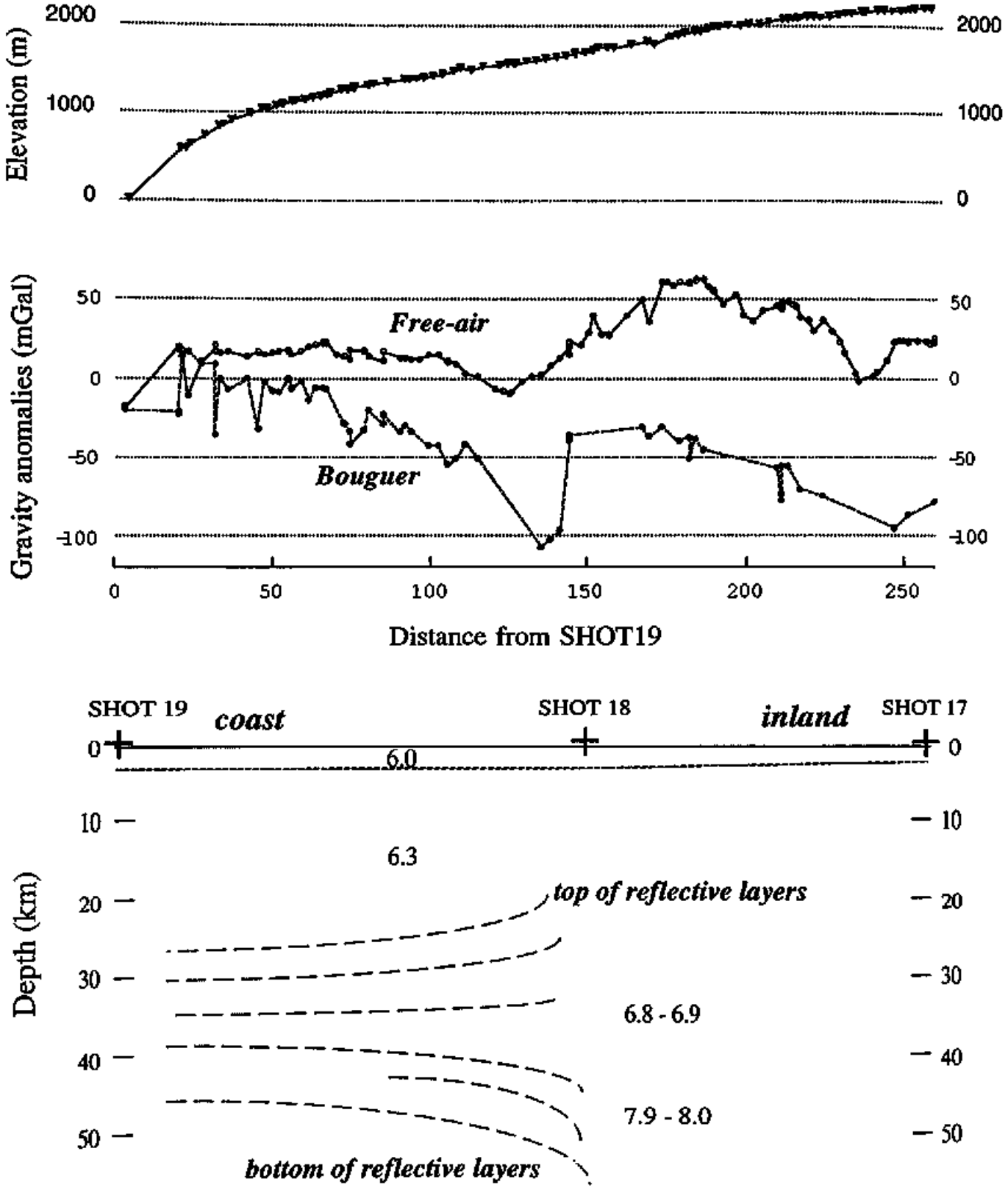

M. Kanao Fig. 14.

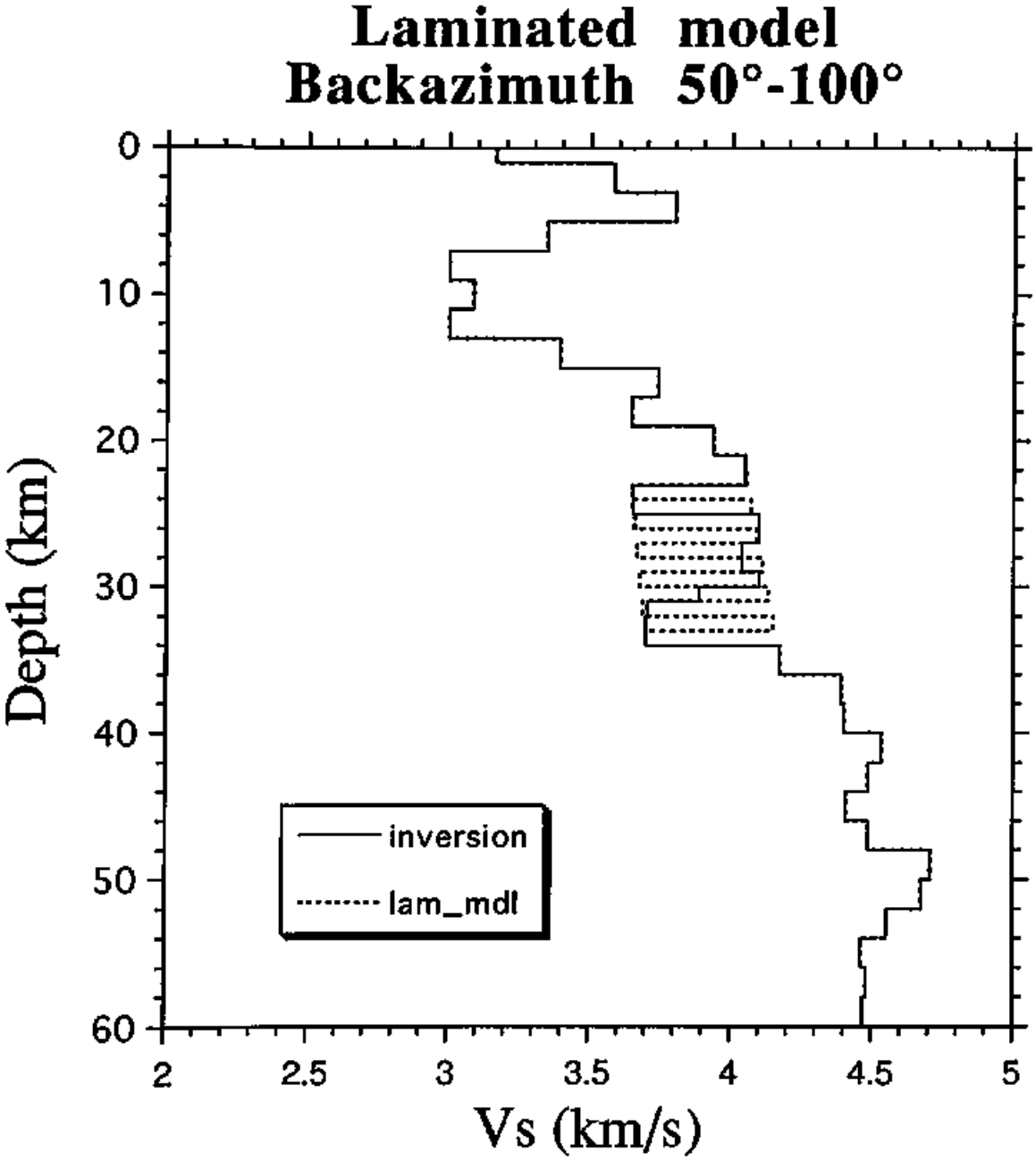

M. Kanao Fig. 15a.

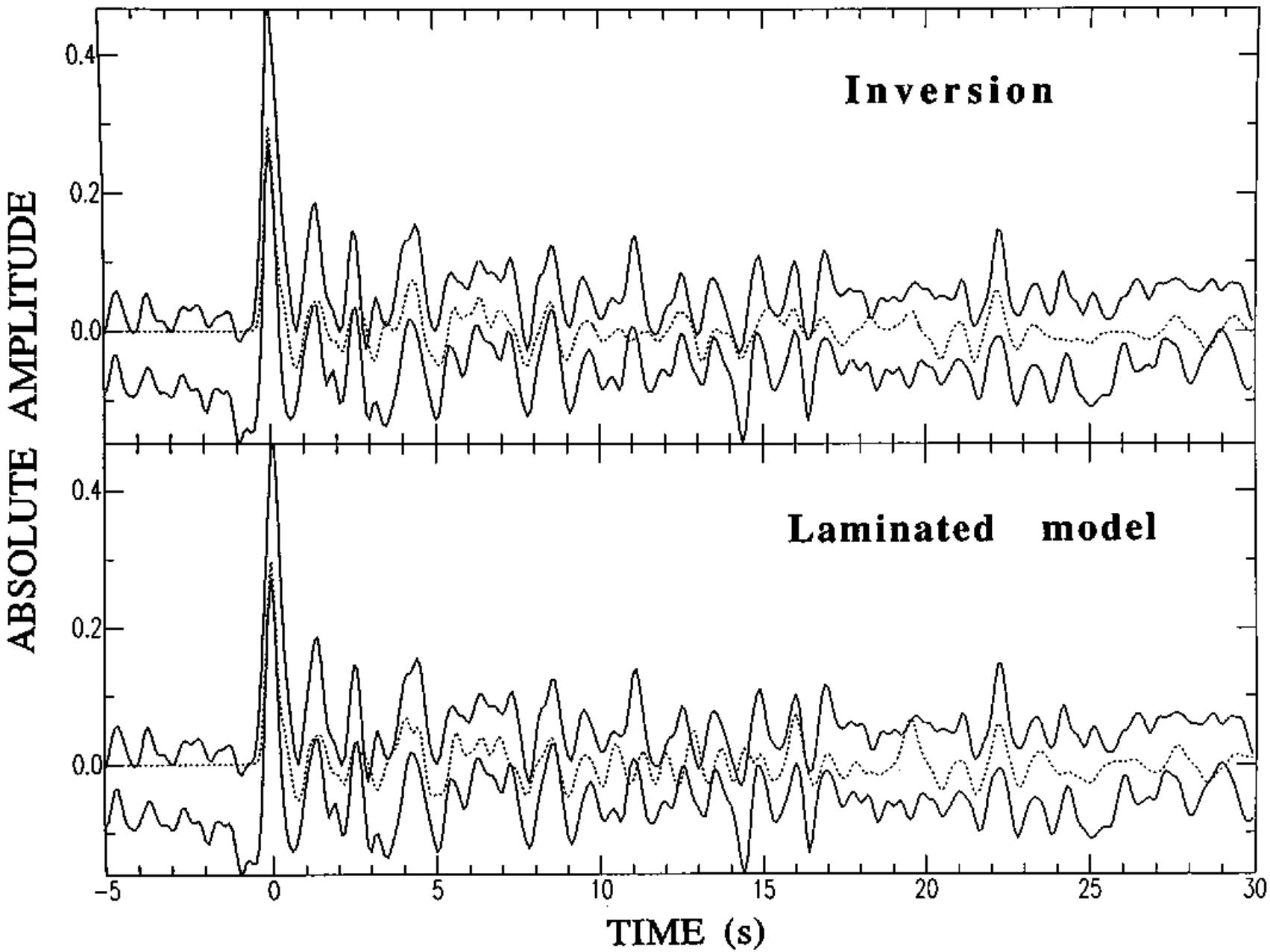

M. Kanao Fig. 15b.

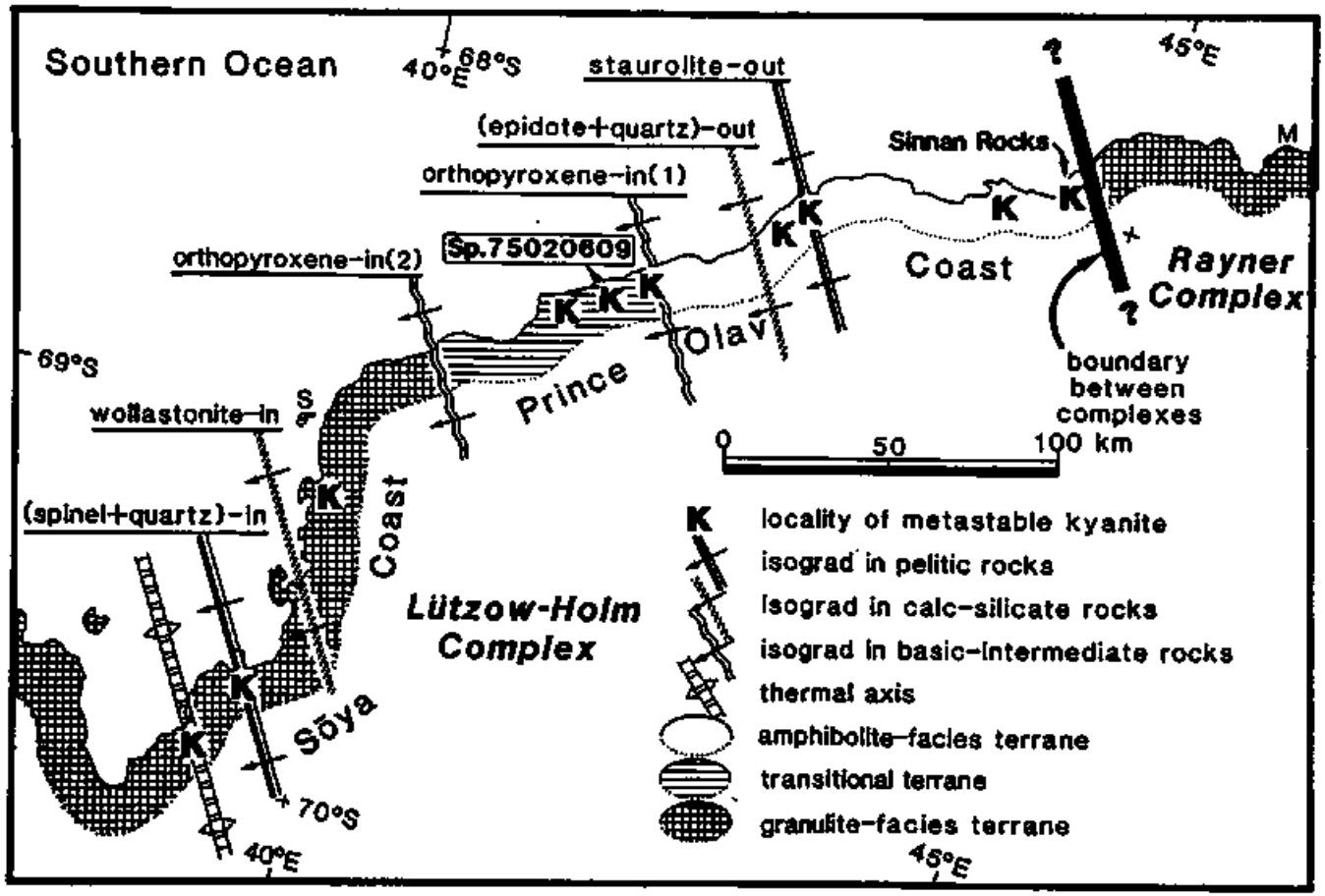

M. Kanao Fig. 16.

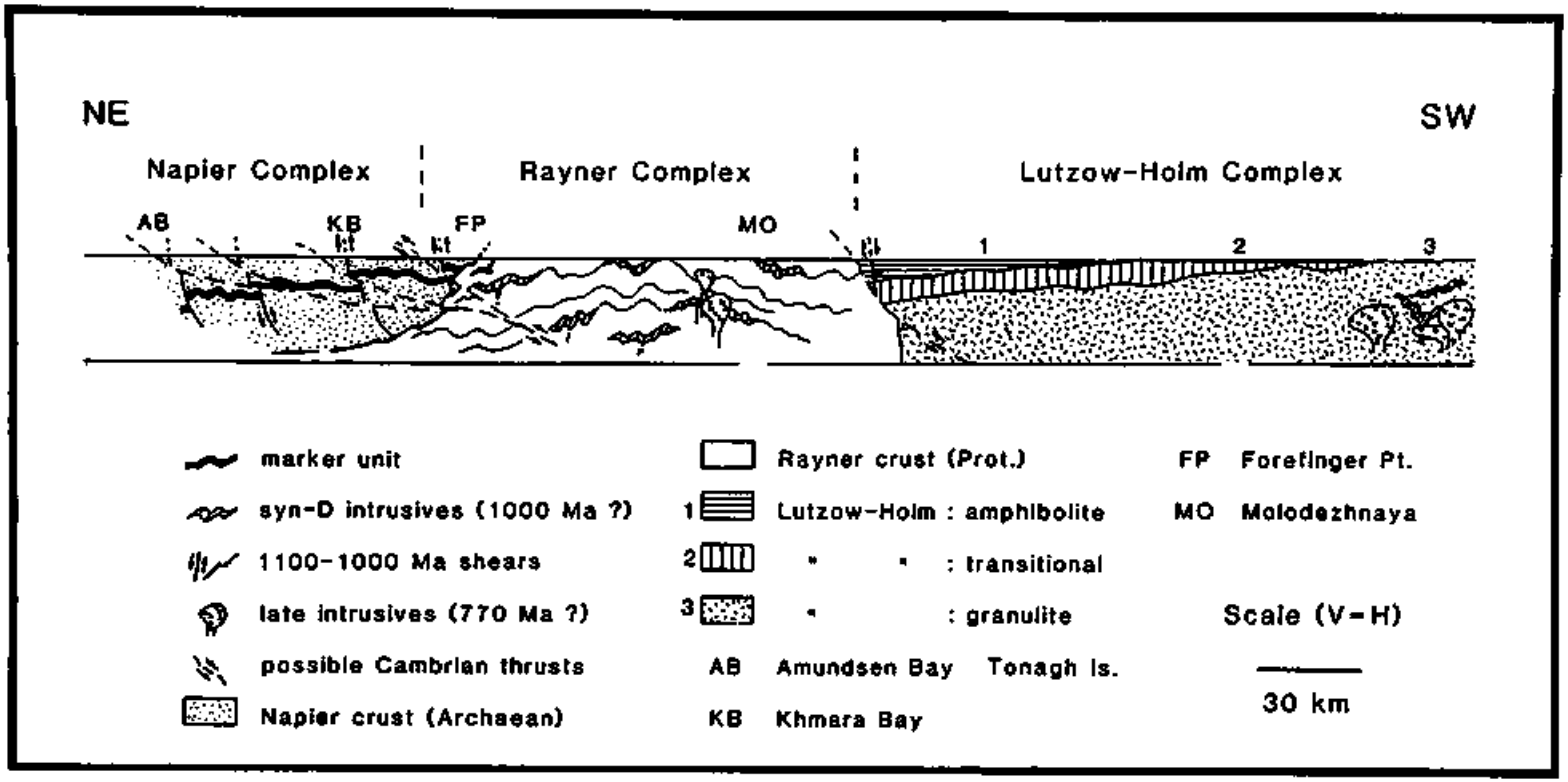

M. Kanao Fig. 17.

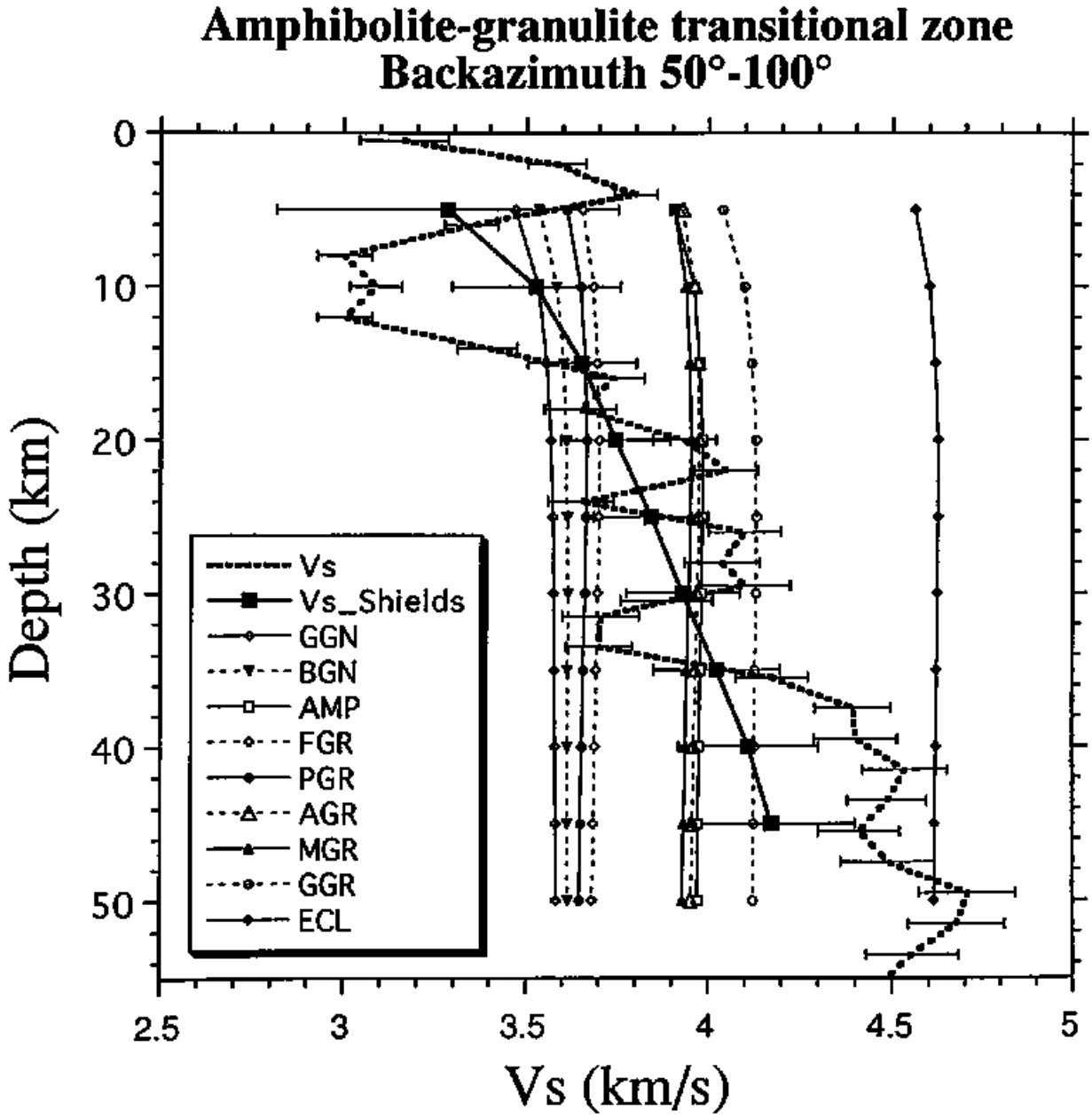

M. Kanao Fig. 18.

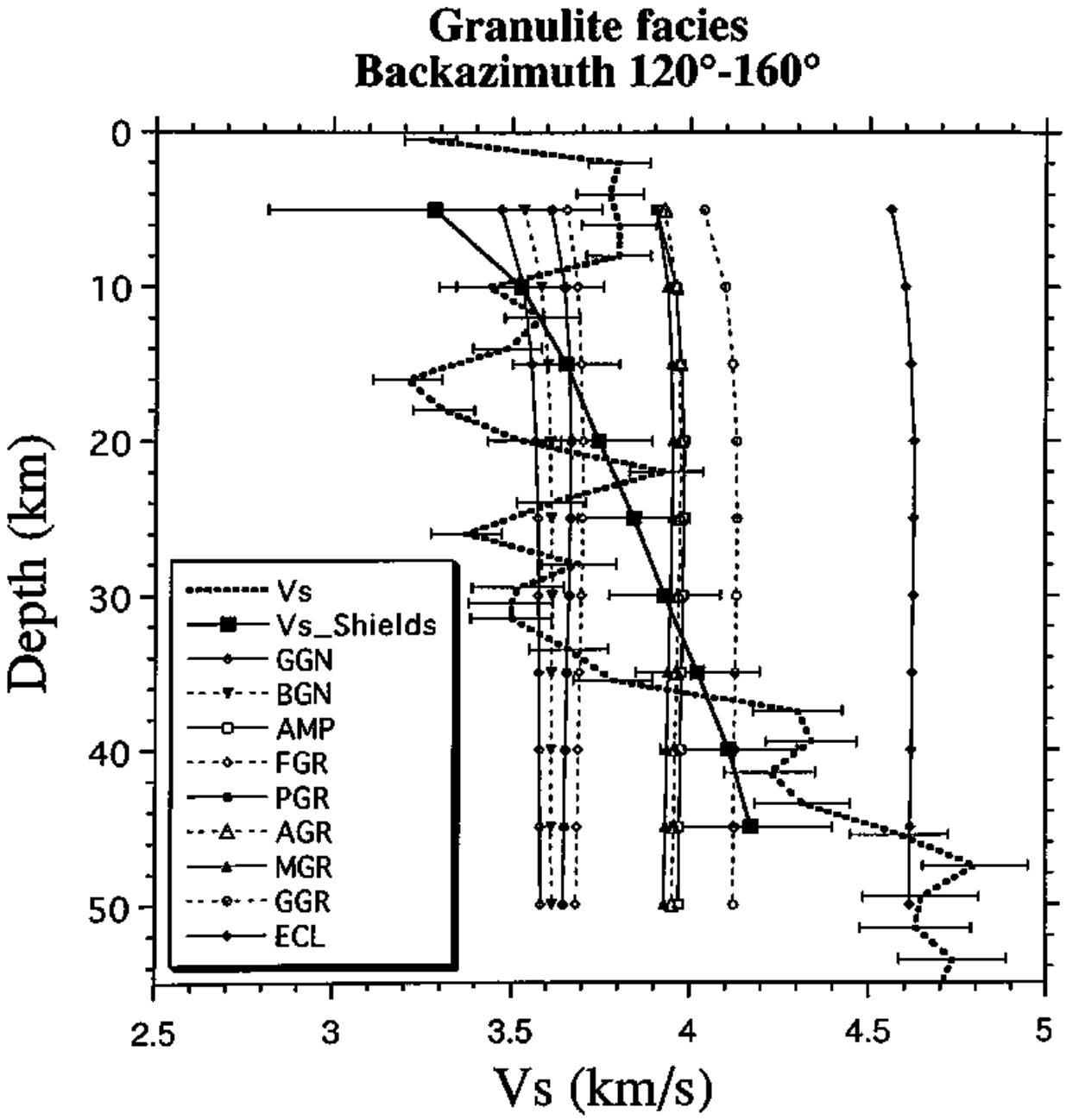

M. Kanao Fig. 18. (continued)

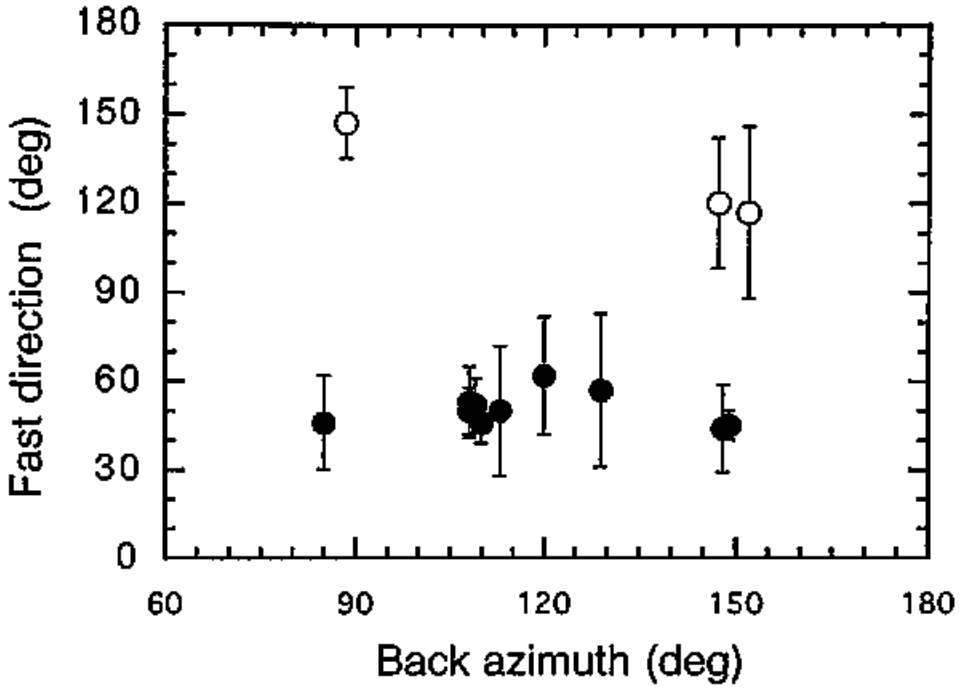

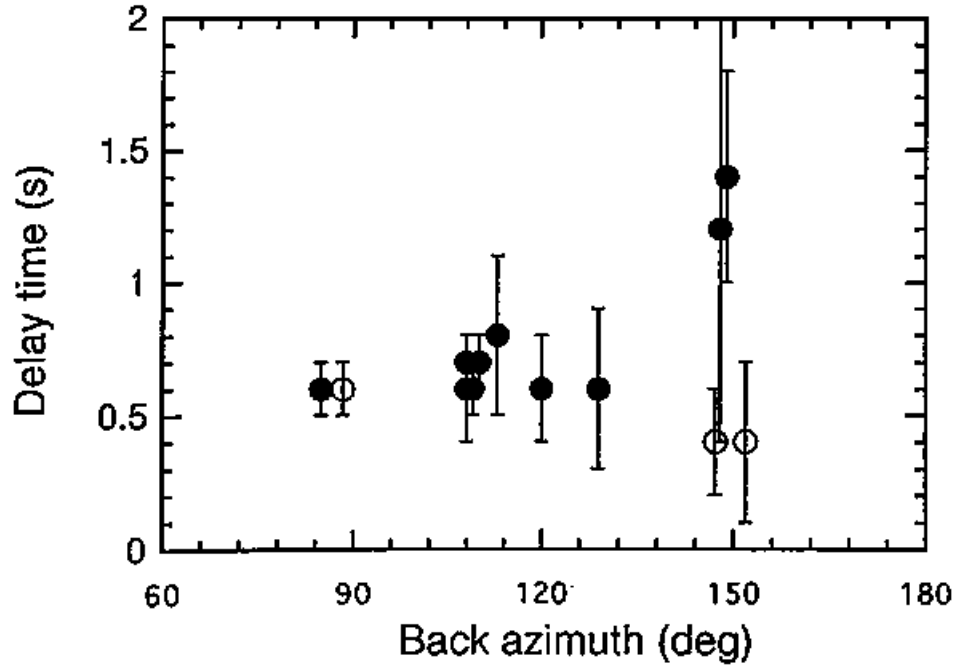

M. Kanao Fig. 19.

Date	Lat. deg.	Lon. deg.	Depth km	Mb	Distance deg.	Backazimuth deg.	Inc.angle deg.	stack_wt.
Amphibolite-Granulite transitional zone								
backazimuth 50°-60°)		*N=4*						
Nov. 18,1990	3.942N	97.343E	67	5.7	82.718	58.274	21.32	0.40
Aug. 26,1991	6.882N	94.609E	22	5.8	84.682	54.774	20.70	0.40
Aug. 07,1992	9.291N	93.479E	66	6.0	86.642	52.995	20.02	0.40
Jan. 20,1993	3.144N	97.633E	68	6.2	82.061	58.798	21.54	0.40
backazimuth 60°-70°)		*N=2*						
Sep. 17,1990	5.917S	103.796E	59	5.7	75.505	67.705	23.71	0.60
July 02,1991	1.068S	99.843E	54	5.8	78.775	62.260	22.65	0.60
backazimuth 70°-80°)		*N=2*						
Sep. 02,1992	6.046S	112.138E	625	5.9	78.234	75.760	21.91	0.80
Dec. 27,1992	6.087S	113.050E	601	5.9	78.514	76.642	21.87	0.80
backazimuth 80°-90°)		*N=7*						
May 24,1990	7.363S	120.363E	589	6.4	79.921	84.017	21.46	1.00
May 19,1991	1.156N	122.957E	33	6.0	88.752	83.390	19.28	1.00
May 21,1991	7.517S	126.539E	18	6.2	81.995	89.859	21.64	1.00
June 07,1991	7.204S	122.533E	536	6.2	80.845	85.997	21.26	1.00
June 20,1991	1.196N	122.787E	31	6.2	88.728	83.217	19.29	1.00
Aug. 02,1992	7.126S	121.748E	486	6.2	80.636	85.232	21.42	1.00
Jan. 19,1993	1.221N	126.072E	27	5.8	89.880	86.276	19.12	1.00
backazimuth 90°-100°)		*N=11*						
May 25,1990	2.871S	130.338E	15	5.8	87.666	91.725	19.53	0.80
July 18,1990	6.820S	130.601E	97	5.7	84.100	93.393	20.80	0.80
Dec. 05,1990	5.264S	131.370E	75	5.9	85.818	93.548	20.29	0.80
May 31,1991	6.048S	130.599E	33	6.0	84.815	93.112	20.64	0.80
Aug. 11,1991	3.141S	130.320E	33	5.7	87.409	91.805	19.66	0.80
Aug. 24,1991	6.065S	130.368E	149	5.6	84.716	92.903	20.54	0.80
Oct. 15,1991	6.494S	130.043E	137	5.9	84.202	92.755	20.72	0.80
Oct. 18,1992	6.279S	130.214E	119	5.8	84.462	92.837	20.66	0.80
Nov. 17,1992	5.822S	130.616E	33	5.9	85.030	93.046	20.57	0.80
Dec. 23,1992	6.541S	130.417E	102	6.1	84.292	93.121	20.73	0.80
Jan. 20,1993	7.205S	128.566E	33	6.2	82.908	91.637	21.30	0.80
Granulite facies								
backazimuth 120°-130°)		*N=4*						
Oct. 12,1991	13.742S	166.673E	44	5.9	89.490	129.195	19.16	0.60
Mar. 03,1992	14.384S	167.179E	148	5.9	89.019	129.848	19.17	0.60
Sep. 15,1992	14.053S	167.269E	184	6.3	89.359	129.838	19.12	0.60
Oct. 15,1992	14.537S	166.711E	25	6.2	88.743	129.457	19.28	0.60
backazimuth 130°-140°)		*N=10*						
July 27,1990	15.355S	167.464E	126	6.4	88.171	130.388	19.32	0.80
Aug. 10,1990	20.199S	168.328E	47	5.8	83.779	132.549	20.98	0.80
Aug. 12,1990	19.435S	169.132E	140	6.3	84.721	133.065	20.55	0.80
Dec. 23,1990	15.182S	167.386E	143	5.6	88.314	130.266	19.28	0.80
Aug. 14,1991	13.593S	167.607E	14	6.1	89.891	130.022	19.12	0.80
Aug. 15,1991	16.064S	168.010E	171	5.9	87.643	131.092	19.39	0.80
Oct. 17,1992	19.226S	169.553E	12	5.8	85.031	133.390	20.59	0.80
Oct. 19,1992	19.385S	169.593E	21	5.7	84.889	133.470	20.63	0.80
Nov. 04,1992	14.238S	167.641E	14	6.1	89.285	130.236	19.20	0.80
Dec. 08,1992	15.483S	168.012E	34	5.7	88.198	130.931	19.37	0.80
backazimuth 140°-150°)		*N=22*						
June 23,1990	21.568S	176.483W	181	6.4	85.979	146.693	20.12	1.00
June 29,1990	21.552S	179.332W	616	5.7	85.415	144.096	19.46	1.00
July 22,1990	23.622S	179.893W	531	5.9	83.290	144.063	20.46	1.00
Aug. 21,1990	33.373S	178.046W	33	5.7	74.196	147.948	24.18	1.00

Date	Lat. deg.	Lon. deg.	Depth km	Mb	Distance deg.	Backazimuth deg.	Inc.angle deg.	stack_wt.
Dec. 21,1990	20.467S	174.161W	13	6.1	87.497	148.592	19.63	1.00
Jan. 08,1991	18.057S	173.534W	33	6.1	89.965	148.696	19.10	1.00
Apr. 18,1991	22.924S	179.342W	471	5.7	84.082	144.399	20.32	1.00
June 09,1991	20.252S	176.218W	266	6.1	87.312	146.658	19.39	1.00
Sep. 30,1991	20.878S	178.591W	566	6.3	86.224	144.620	19.34	1.00
Oct. 18,1991	24.295S	177.561W	198	5.8	83.114	146.307	21.01	1.00
Aug. 18,1992	28.644S	178.324W	201	5.6	78.737	146.608	22.46	1.00
Sep. 09,1992	23.509S	178.877W	554	5.3	83.137	142.932	20.46	1.00
Sep. 09,1992	31.327S	177.299W	33	5.1	76.327	148.109	23.47	1.00
Oct. 24,1992	29.536S	177.279W	19	5.8	78.073	147.720	22.91	1.00
Oct. 24,1992	29.944S	177.113W	10	5.1	77.707	147.956	23.04	1.00
Oct. 24,1992	30.090S	177.215W	10	5.5	77.546	147.900	23.10	1.00
Oct. 25,1992	29.900S	177.352W	26	5.7	77.704	147.739	23.03	1.00
Oct. 29,1992	35.813S	179.672W	54	5.1	71.515	147.181	25.02	1.00
Nov. 12,1992	22.401S	178.104W	360	5.9	84.845	145.401	20.24	1.00
Dec. 26,1992	32.457S	178.282W	10	5.5	75.041	147.531	23.92	1.00
Dec. 31,1992	32.015S	178.025W	16	5.8	75.519	147.646	23.75	1.00
Jan. 04,1993	22.055S	174.866W	33	5.9	85.594	148.267	20.31	1.00
backazimuth 150°-160°)		*N=1*						
Dec. 11,1991	23.368S	171.044W	37	5.8	81.446	151.993	21.78	0.80
Lützow-Holm Bay								
backazimuth 210°-220°)		*N=2*						
Aug. 21,1990	27 487S	104.266W	11	6.0	80.141	212.096	22.24	0.40
June 23,1992	36.104S	101.220W	10	5.6	71.182	212.682	25.19	0.40
backazimuth 240°-250°)		*N=7*						
Sep. 02,1990	23.852S	70.484W	43	4.7	74.734	242.985	23.96	1.00
Oct. 31,1990	26.634S	70.481W	60	5.5	72.140	241.968	24.78	1.00
June 23,1991	26.802S	63.349W	558	6.4	69.656	248.188	24.71	1.00
June 21,1992	26.503S	70.659W	39	5.7	72.319	241.860	24.76	1.00
Aug. 20,1992	26.177S	69.088W	105	5.4	72.120	243.364	24.73	1.00
Oct. 10,1992	26.013S	70.730W	34	5.2	72.798	241.978	24.61	1.00
Dec. 23,1992	19.766S	68.808W	106	5.4	78.001	245.951	22.81	1.00
backazimuth 300°-310°)		*N=3*						
July 14,1990	0.003N	17.376W	11	6.2	78.649	301.261	22.74	0.10
Aug. 05,1990	1.080S	13.887W	10	5.6	76.570	304.332	23.42	0.10
Sep. 21,1992	7.816S	13.585W	10	5.8	70.095	302.522	25.54	0.10
backazimuth 350°-360°)		*N=5*						
May 20,1990	5.121N	32.145E	15	6.7	74.189	352.294	24.20	1.00
May 24,1990	5.277N	31.829E	17	5.9	74.360	351.976	24.14	1.00
May 24,1990	5.358N	31.848E	16	6.5	74.439	351.999	24.12	1.00
July 09,1990	5.395N	31.654E	13	5.9	74.485	351.801	24.10	1.00
Oct. 09,1991	1.804N	31.293E	33	5.7	70.940	351.226	25.24	1.00

Layer No.	Thickness km	Initial km/s	Lower-limit km/s	Upper-limit km/s	Vp/Vs	Qp	Qs
1	1.00	3.47	2.50	3.80	1.73	60	25
2	2.00	3.53	3.00	3.80	1.73	120	50
3	2.00	3.58	3.00	3.80	1.73	145	60
4	2.00	3.58	3.00	3.80	1.73	157	65
5	2.00	3.61	3.00	3.80	1.73	194	80
6	2.00	3.64	3.00	3.80	1.73	206	85
7	2.00	3.64	3.00	3.80	1.73	206	85
8	2.00	3.70	3.10	4.10	1.73	290	120
9	2.00	3.70	3.10	4.10	1.73	290	120
10	2.00	3.70	3.10	4.10	1.73	290	120
11	2.00	3.70	3.10	4.10	1.73	290	120
12	2.00	3.70	3.10	4.10	1.73	290	120
13	2.00	3.70	3.10	4.10	1.73	290	120
14	2.00	3.70	3.10	4.10	1.73	290	120
15	2.00	3.70	3.10	4.10	1.73	290	120
16	1.00	3.70	3.10	4.10	1.73	290	120
17	1.00	3.84	3.50	4.50	1.73	411	170
18	1.00	3.93	3.50	4.50	1.73	508	210
19	2.00	4.02	3.50	4.50	1.73	726	300
20	2.00	4.02	3.50	4.50	1.73	847	350
21	2.00	4.02	3.50	4.50	1.73	847	350
22	2.00	4.02	3.50	4.50	1.73	847	350
23	2.00	4.41	4.10	4.80	1.80	1360	600
24	2.00	4.41	4.10	4.80	1.80	1360	600
25	2.00	4.41	4.10	4.80	1.80	1360	600
26	2.00	4.41	4.10	4.80	1.80	1360	600
27	2.00	4.47	4.10	4.80	1.80	1360	600
28	2.00	4.47	4.10	4.80	1.80	1360	600
29	2.00	4.47	4.10	4.80	1.80	1360	600
30	2.00	4.47	4.10	4.80	1.80	1360	600
31	2.00	4.47	4.10	4.80	1.80	1360	600
32	2.00	4.47	4.10	4.80	1.80	1360	600

M. Kanao Table 2.